MODELLING GAS-LIQUID FLOW AND LOCAL MASS TRANSFER IN STIRRED TANKS

Pasi Moilanen

MODELLING GAS-LIQUID FLOW AND LOCAL MASS TRANSFER IN STIRRED TANKS

Pasi Moilanen

Dissertation for the degree of Doctor of Science in Technology to be presented with due permission for public examination and debate in Auditorium Ke 2 at Helsinki University of Technology (Espoo, Finland) on the 27th of March, 2009, at 12 noon.

Helsinki University of Technology

Department of Biotechnology and Chemical Technology

Chemical Engineering

Teknillinen korkeakoulu

Biotekniikan ja kemian tekniikan laitos

Kemian laitetekniikka

ABSTRACT

This doctorial thesis offers a guideline for modelling gas-liquid flow in stirred tanks with computational fluid dynamics (CFD). Particularly the effect of varying physical properties and industrial operating conditions is highlighted. The most important thing in modelling mass transfer in stirred vessels is the accurate prediction of local bubble size. Population balances for bubbles are needed for accurate description of the local mass transfer rate. There are many pitfalls in gas-liquid modelling at the transitional turbulence regime, and they need to be recognised and dealt with at a reasonable computational cost. Details of the work are presented in the included publications, this thesis sums up the findings.

Backbone of this thesis is the experimental work done on 14 and 200 dm^3 vessels. Experimental techniques were compared in making bubble size distribution (BSD) measurements. A variety of experiments were made to investigate: physical properties, vapour-liquid equilibrium, gas hold-up, gas-liquid mass transfer, bubble size distributions, local mixing times, flow fields and bubble swarm interactions.

Parameters for a number of phenomenological models were fitted with a computationally less demanding multiblock model and were then used to simulate stirred reactors with CFD. The early systems were lean dispersions of low viscosity; at the end of this work opaque shear thinning G-L dispersions were modelled. The effect of impeller geometry on G-L mass transfer was studied by simulating three impeller geometries. There were no differences in the volumetric mass transfer rate between the impellers, although the flow patters and gas hold-up showed clear differences between the impellers. Heterogeneous behaviour like gas slug creation and reactor dead-spaces were successfully modelled. The simulated dispersions were highly heterogeneous: 50% of mass transfer took place in less than 10% of the reactor volume. A xanthan fermentation batch lasting for days was modelled; the reaction speed was bottlenecked by both mixing and mass transfer. These findings strongly support the use of spatially detailed models over ideal mixing assumption.

TIIVISTELMÄ

Tämä väitöskirja toimii ohjenuorana kaasu-neste aineensiirron mallintamiselle sekoitussäiliöissä tietokonepohjaisella virtauslaskennalla (CFD). Etenkin aineominaisuuksien ja reaktorien teollisten operointiolosuhteiden merkitystä korostetaan. Tärkein asia mallinnettaessa kaasu-neste aineensiirtoa on paikallisen kuplakoon ennustaminen. Paikallisen aineensiirtonopeuden tarkkaan mallintamiseen tarvitaan populaatiotase kuplille. Etenkin turbulenssin mallintaminen transitioalueella, jossa virtaus ei ole laminaaria eikä turbulenttia on haastavaa. Ongelmatilanteet on tunnistettava ja ratkaistava mahdollisimman pienellä laskentateholla. Tässä väitöskirjassa ei mennä pitkälle yksityiskohtiin, tarkoituksena on lähinnä koota yhteen osajulkaisujen tulokset.

Koko väitöskirja tukeutuu pitkälti koetoimintaan laboratoriomittakaavassa 14 ja 200 litran sekoitussäiliöissä. Mittaustekniikoita vertailtiin kuplakokojakaumien (BSD) mittauksessa. Koetoiminnassa pyrittiin tutkimaan aineominaisuuksia, höyry-neste tasapainoja, kaasuosuuksia, kaasu-neste aineensiirtoa, kuplakokojakaumia, paikallisia sekoitusaikoja, virtauskenttiä ja kuplaparven vuorovaikutusta.

Ilmiömalleissa käytetyt parametrit sovitettiin laskennallisesti kevyellä monilohkomallilla, sovitetuilla yhtälöillä laskettiin tämän jälkeen sekoitussäiliöitä CFD:llä. Simuloinnit ja mittaukset aloitettiin laimeilla ja yksinkertaisilla vesi-ilma dispersioilla. Lopulta päädyttiin mallintamaan ja mittaamaan leikkausohenevia, sakeita ja läpinäkymättömiä kaasu-neste dispersioita. Työssä tutkittiin kolmen eri sekoittimen vaikutusta kaasu-neste aineensiirtoon. Aineensiirtonopeudessa ei ollut eroavaisuuksia vaikka eri sekoittimilla oli selkeä vaikutus virtauskenttiin ja kaasuosuuteen. Sekoitusreaktorien heterogeenisyys osoitettiin simuloimalla onnistuneesti reaktorin kuolleita alueita ja kaasupullahduksia. Aineensiirrosta tapahtuu jopa puolet tapahtuu hyvin pienellä alueella (10% reaktoritilavuudesta) sekoittimen läheisyydessä. Useita päiviä kestävästä teollisesta ksantaanin panosreaktiosta tehtiin simulointi, joka osoitti että reaktionopeutta rajoittavat sekä sekoitusolosuhteet ja kaasu-neste aineensiirto. Väitöskirjassa esitetyt tulokset tukevat osoittavat selvästi että paikallisella mallintamisella saadaan parempia tuloksia kuin ideaalisekoitus-oletuksella.

PREFACE

This thesis was started in 2003 at Helsinki University of Technology, Laboratory of Chemical Engineering and Plant Design.

First I want to thank Professors Juhani Aittamaa and Ville Alopaeus for providing me with this thesis and a good learning environment for scientific research. They have forever imprinted my mind with the importance of physical modelling instead of empirical correlations.

Co-authors Marko Laakkonen, Olli Visuri, Petri Uusi-Kyyny, Juha-Pekka Pokki, Minna Pakkanen, Tatu Miettinen, Kari Saari, Markus Honkanen and Pentti Saarenrinne are acknowledged for their contribution. I want to thank our laboratory's staff in general for creating a great working environment, Lasse Westerlund and Sirpa Aaltonen have kept things running as smoothly as possible. A special thanks for inspiration and scientific diligence goes to Marko Laakkonen for his enfusiasm with small bubbles.

Asta Nurmela, Olli Visuri, Suvi Jussila and Elina Nauha have made this thesis possible by providing accurate measurements. The financial support of TEKES and our industrial partners is gratefully acknowledged.

 Finally and most importantly I want to thank my parents for making all of this possible.

Tampereella 2.2.2009

Pasi Moilanen

LIST OF PUBLICATIONS

This thesis is based on the following publications (Appendices I-IX), which are referred to in the text by their roman numerals

[I]   Moilanen, P., Uusi-Kyyny, P., Pokki, J-P., Pakkanen, M., Aittamaa, J., Vapour Liquid Equilibrium for Butane + Methanol, +Ethanol, +2-Propanol, +2-Butanol and +2-Methyl-2-Propanol (TBA) at 323 K. *J. Chem. Eng. Data* (**2008**), 53(1), 83-88.

[II]   Laakkonen, M., Moilanen, P., Miettinen, T., Saari, K., Honkanen, M., Saarenrinne, P., Aittamaa, J. Local bubble size distributions in agitated vessel. Comparison of three experimental techniques. *Chem. Eng. Res. Des.* (**2005**), 83(A1), 50-58.

[III]   Moilanen, P., Laakkonen, M., Aittamaa, J., CFD modelling of local bubble size distribution in agitated gas-liquid vessels – Verification against experiments, European Symposium on Computer-Aided Process Engineering - 14, Portugal (**2004**), 241-246.

[IV]   Moilanen, P., Laakkonen, M., Aittamaa, J., Modeling aerated fermenters with computational fluid dynamics. *Ind. Eng. Chem. Res.* (**2006**), 45(25), 8656-8663.

[V]   Laakkonen, M., Moilanen, P., Alopaeus, V., Aittamaa, J. Dynamic modeling of local reaction conditions in an agitated aerobic fermenter. *AIChE J.* (**2006**), 52(5), 1673-1689.

[VI]   Laakkonen, M., Moilanen, P., Alopaeus, V., Aittamaa, J. Modelling local bubble size distributions in agitated vessels. *Chem. Eng. Sci.* (**2007**), 62(3), 721-740.

[VII]   Laakkonen, M., Moilanen, P., Alopaeus, V., Aittamaa, J. Modelling local gas-liquid mass transfer in agitated vessels. *Chem. Eng. Res. Des.* (**2007**), 85(A5), 665-675.

[VIII]   Moilanen, P., Laakkonen, M., Visuri, O., Aittamaa, J. Modelling local gas-liquid mass transfer in agitated viscous shear-thinning dispersions with CFD. *Ind. Eng. Chem. Res.* (**2007**), 46(22), 7289-7299.

[IX]   Moilanen, P., Laakkonen, M., Visuri, O., Alopaeus, V., Aittamaa, J., Modelling mass transfer in an aerated 0.2 m^3 vessel agitated by Rushton, phasejet and combijet impellers. *Chem. Eng. J.* (**2008**), 142, 95-108.

AUTHOR CONTRIBUTION

[I]   The author wrote the paper, made the regressions and analysed the results.

[II]   The author helped with analysing the results and making the conclusions

[III]   The author wrote the paper, made the simulations and analysed the results.

[IV]   The author wrote the paper, made the simulations and analysed the results.

[V]   The author selected the bioreaction and model system, made the CFD-simulations and helped in writing the article.

[VI]   The author made the CFD-simulations and helped in writing the article.

[VII]   The author made the CFD-simulations and helped in writing the article.

[VIII] The author wrote the paper, made the simulations and analysed the results.

[IX]   The author wrote the paper, made the simulations and analysed the results.

_____   _____

Pasi Moilanen   Ville Alopaeus

Espoossa 4.2.2009

TABLE OF CONTENTS

1. INTRODUCTION

Stirred reactors are among the most widely used reactors in chemical industries. They offer unmatched flexibility and control over transport processes occurring in the reactor (Ranade, 2002). However, detailed understanding of the local phenomenon in the reactor is still often replaced by empirical correlations. Alone in the US chemical industry the yearly cost of inadequate mixing is estimated to be from $1 billion to $10 billion (Paul *et al*., 2004). Gas-Liquid mass transfer is often the reaction rate limiting factor, especially when dealing with slightly soluble gasses (Schügerl and Bellgard, 2000).

Traditionally stirred tanks haven been designed with dimensionless correlations which treat the vessel as ideally mixed. These correlations are only reliable with similar reactor geometry and operating conditions. This approach may not be adequate to describe and scale-up complex systems like fermentation froths, which often exhibit viscous non-Newtonian behaviour. In large fermenters the conditions are seldom homogeneous (Schügerl and Bellgard, 2000; Gogate *et al*., 2000). Cavern formation is common with shear-thinning fluids (Nienow and Elson, 1988; Amanullah *et al*., 1998a; Amanullah *et al*., 1998b). If the mixing is inadequate there might be problems with low dissolved oxygen and the distribution of nutrients (Hristov *et al*., 2001; Vlaev *et al.*, 2000). Large industrial reactors are often operated in the transitional turbulence regime, where the flow is neither laminar nor fully turbulent.

Phenomenological models are independent of vessel geometry and operating conditions, allowing high scale-up ratios (Bisio and Kabel, 1985). The models are solved based on local physical properties (e.g viscosity, density, pressure, temperature and concentration), and local fluid flow (e.g. turbulence dissipation and shear-rate). With computational fluid dynamics (CFD) it is possible to calculate the local flow field in great detail. In this work phenomenological models are used to investigate gas-liquid flow and mass transfer in stirred vessels. The aim of this work is to develop tools for G-L reactor design, operation and scale-up. Even small improvements in reactor performance can result in considerable savings.

There is a need to validate the phenomenological models like population balances (PB) for bubbles with breakage and coalescence, before complex gas-liquid simulations can be trusted. This is easier to do with simpler systems that can be studied in laboratory vessels (i.e. lean air-water dispersions). Various experiments were carried out to provide data for model validation at laboratory scale. The closure model parameter fitting is far too computationally demanding with CFD, so a lighter multiblock model was used in the fitting (Laakkonen, 2006). The verified models were then used to simulate gas-liquid reactors with CFD to gain insight on how industrial reactors function (Figure 1).
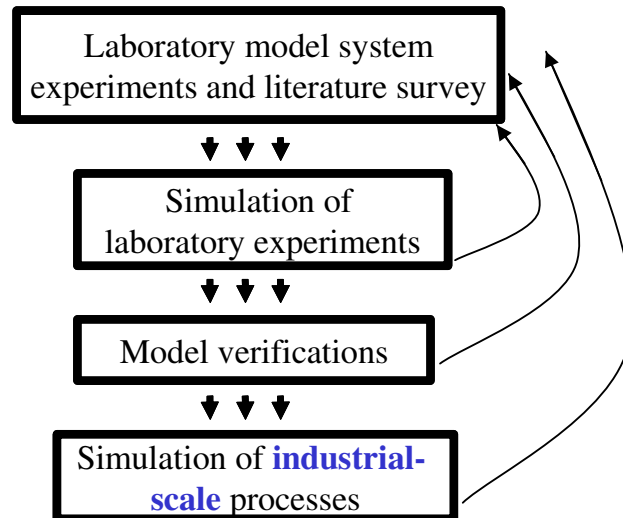
Figure 1. The modelling strategy.

Local phase equilibrium sets the final value for mass transfer. In paper [I] vapour liquid equilibrium (VLE) is investigated from n-butane – alcohol systems. Three measurement techniques for local bubble size determination are compared in article [II]. In paper [III] local BSDs (Bubble Size Distributions) are investigated in CO_2-n – butanol and air-water dispersions at low gassing rates. The investigation is widened to denser dispersions and CFD is compared against multiblock model in paper [VI]. G-L mass transfer is modelled in air-water dispersions in paper [VII] and in paper [IX] the effect different impellers on mass transfer is investigated. Papers [IV, V and VIII] sum up the achievements of this thesis. Various aspects of non-Newtonian G-L modelling, bioreaction and scale-up effects are investigated in [IV]. Population balances for bubbles are included in [VIII] and finally the CFD results are used is a multiblock model and batch fermentation strategies are investigated in [V]. In papers [IV and V] large fermenters are investigated in industrial operating conditions.

2. EXPERIMENTAL

Experimental measurements are needed to validate complex sub-models. CFD can predict fairly accurately turbulent or laminar Newtonian one-phase flows. But when dealing with non-Newtonian flow, phase interactions or turbulence in the transitional flow regime further development is needed. Local information is scarce from vessels operating in industrial operating conditions and with real reactor fluids. Dense two-phase dispersions are often opaque, limiting the usefulness of various optical measurement techniques [II] like PIV (Particle imaging velocimetry), photography, PDA (Phase Doppler anemometry), LDA (Laser Doppler anemometry). So, often models need to be validated indirectly based on vessel averaged (global) measurements. For detailed description of G-L mass transfer rate, gas hold-up, mass transfer area and mass transfer rate in the liquid film (k_L) need to be locally modelled. To illustrate that we are dealing with a complex system dependencies between phenomena affecting mass transfer in multiphase flow are illustrated in Figure 2.
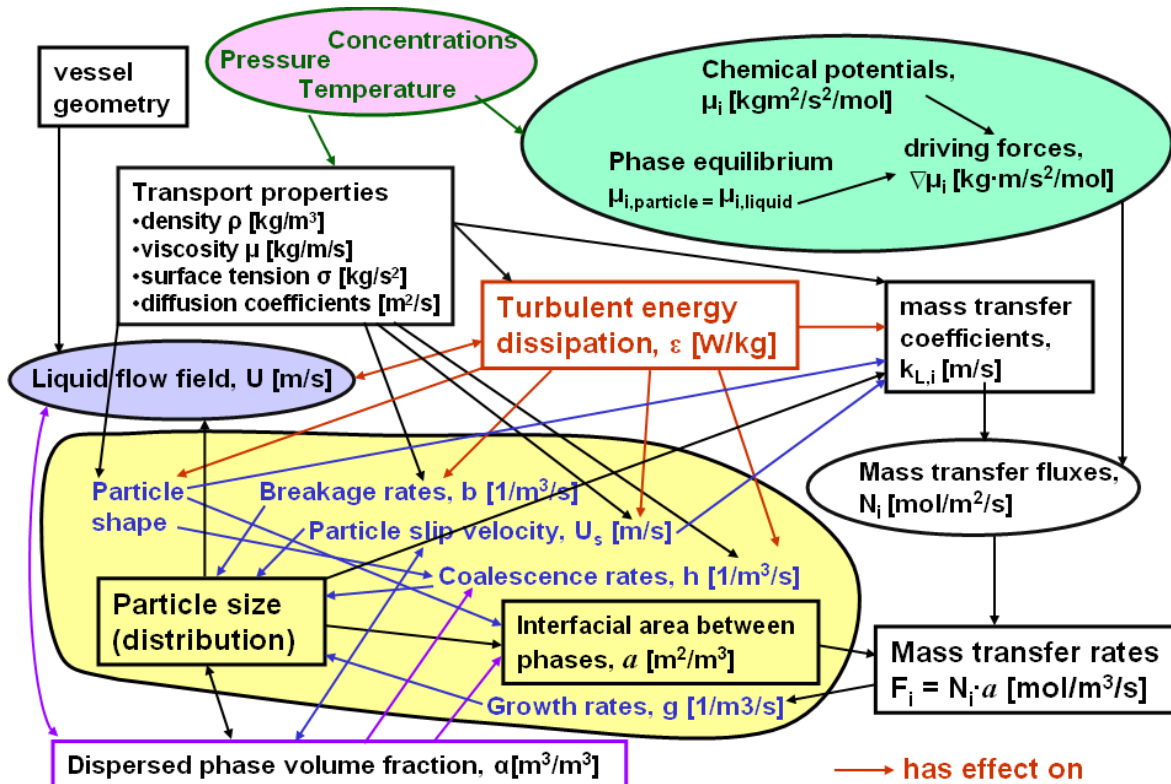
Figure 2. Sub-model interactions in G-L mass transfer modelling, this is the reason why simple correlations often fail.

2.1 Experimental setup and systems

Majority of the measurements were carried out in geometrically similar 14 and 200 dm^3 laboratory vessels. The 14 dm^3 vessel dimensions are presented in Figure 3a. Two different vessel sizes allow the investigation of scale-up effects. Experimental systems included air – water, CO_2 – butanol and air – aqueous xanthan. These systems cover a range of varying physical properties (viscosity, density and surface tension). In papers [II-III] the dispersion was lean to allow a wider range of experimental techniques to be used. In papers [IV-IX] the operating

conditions are more in-line with industrial agitated G-L reactors, gassing rate (0.1-1.0 vvm) and mixing intensity (0.1-3.0 W/kg(liquid)). When scaling up reactors the model needs to accurately describe the effect of vessel geometry. Thus, three different impellers were compared; the investigated impellers are presented in Figure 3b. The impeller diameters (D_{imp}) are Rushton (RT) = T/3, Phasejet (PJ) = 0.44·T and Combijet (CJ) =0.46·T. The experiments included: physical properties of the fluid (surface tension, viscosity and density), gas hold-up, mixing intensity, local mixing times, local flow fields, dissolved oxygen, bubble rise velocities and especially the local BSDs. The VLE measurements [I] were carried out in a static total pressure apparatus (Uusi-Kyyny et al. 2002).
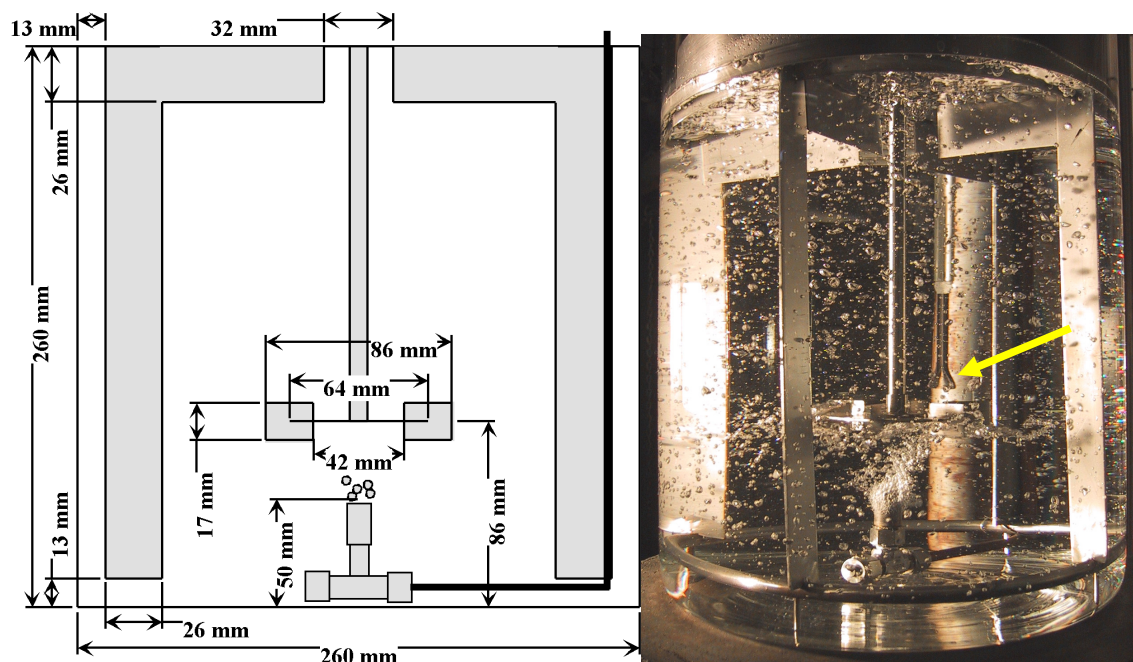
Figure 3a. The 14 dm^3 vessel dimensions, dimensions of the 194 dm^3 are obtained by multiplying with 2.423. In the picture the capillary suction probe is indicated with an arrow.


Figure 3b. The impellers: Combijet (CJ), Phasejet (PJ) and Rushton (RT).

2.2 Bubble size distributions

There exist a number of methods capable of investigating local bubble size distributions. Here the BSDs are measured with three potential methods: capillary suction probe (CSP), digital photography (DI) and phase Doppler anemometry. Experimental local BSDs offer us a way to validate complex phenomenological models.

Digital photography: The most informative of the available measurement techniques is photography, since the results can be visually evaluated. The method is non-intrusive and optical. Post processing of the results is the most demanding part of digital photography, which can be either manual or automated. In the automated image analysis [II] 10000 bubbles were measured, this required in each experiment from 500 to 2000 pictures from a control area of 17 x 21.2 mm in lean air-water experiments and 12 x 15 mm in lean CO_2-n-butanol experiments. Calibration of digital imaging was made by placing a ruler in the dispersion and taking a picture of it. Davis 6.2.2 (LaVision) program was used to identify bubbles from the pictures. Identification was made based on the threshold method (Chigier, 1991). It identifies the main axes of a bubble from the background based on the colour shades. BSDs were measured manually from xanthan solutions [IV,V,VII]. Due to dense dispersion photographing was possible only near the vessel wall. The BSDs were analysed by identifying 500-1500 bubbles manually as ellipsoids. The particle analysis tool ImageJ 1.32 freeware was used to convert the ellipsoids from the thresholded images to BSDs. The resolution of digital camera allowed the detection of larger than ~0.1 mm (5 pixel) bubbles. In Figure 4 typical pictures from automated and manual BSD determination are presented.
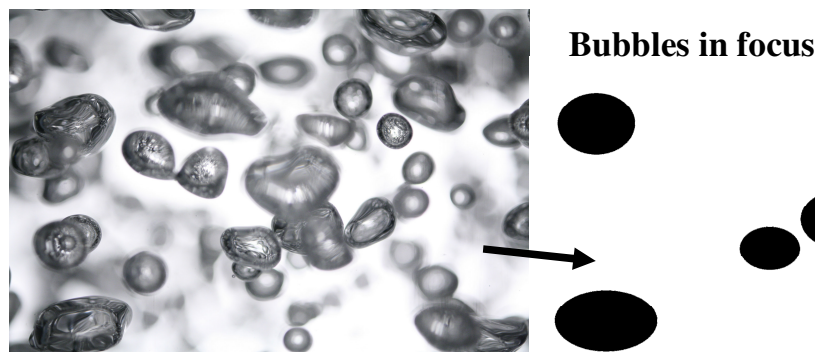
Bubbles in focus

Figure 4. Manual analysing of bubbles. In left the raw data, on right the focused bubbles are manually selected out as ellipsoids and then analysed automatically. This procedure is repeated many times to get a statistically relevant BSD.

Capillary suction probe: A Hydromess apparatus was used in the measurements. In this method a bubble is sucked into a capillary (Figure 5) and the length of the slug is identified by photoelectric probes, then the volume of the slug is calculated and the corresponding bubble size is recorded. The CSP is an intrusive pointwise technique that limits its use in small vessels. The CSP can be used in opaque dispersions and even with high hold-ups (<25 vol-%). The measurable bubble size is 1-5 times the capillary diameter, giving a 0.4…8 mm measurement range [II] Barigou and Greaves (1992ab).
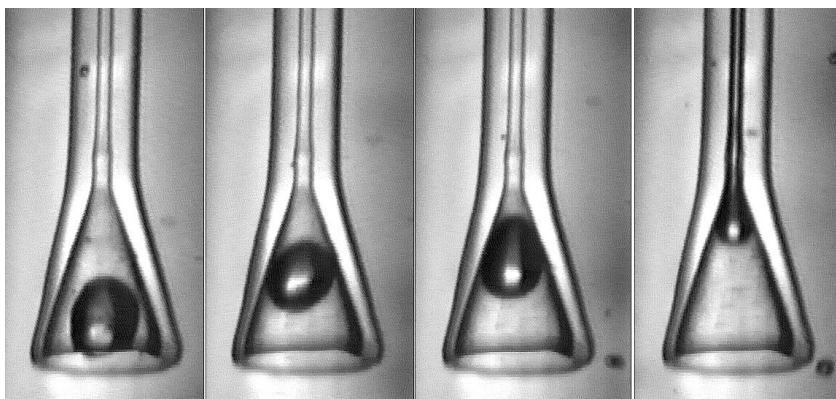
Figure 5. Capillary suction probe in action.

Phase Doppler anemometry: The PDA is a pointwise non-intrusive technique that is based on light scattering theory. The method determines bubble size based on the curvature of the bubble, this method is limited to spherical bubbles in lean dispersions.

2.3 Fluid flow fields

Particle imaging velocimetry is a method where tiny tracer particles in the fluid flow are photographed as image pairs. Then the local fluid velocity is calculated based on the displacement of the particles between the image pair. The particles are illuminated by a light sheet generated by a high intensity laser. Since the timescales that we are dealing with are so fast, our exposure times are in order of 5ms. Principles of the method can be found in (Westerweel, 1997; Paul *et al*., 2004; Adrian, 2005). The method is indirect and is hindered by optical disruptions, making it hard to use with opaque dispersions. However it's one of the most suitable techniques to determine local flow fields that are a key component in model validation. The PIV apparatus and software (davis flowmaster 7.0) were made by LaVision. The results presented in this work are 2D-PIV. The 14 dm^3 glass vessel was placed in a rectangular bath to eliminate optical distortions and all the metal surfaces were painted black to eliminate reflections.

2.4 Local mixing times

Local mixing times were measured from aqueous xanthan solutions in order to verify single-phase CFD simulations. The local mixing time is calculated from the colour change in the liquid, based on the spread of an inert food dye. The method is similar to the work of Cabaret *et al*. (2006) and is presented in detail in Visuri *et al.* (2007). A digital video camera (Panasonic AW-E330A) was used to identify the degree of mixing based on colour change, the experimental area is a ¼ segment of the vessel. The dye was pneumatically injected trough a metal pipe into the impeller discharge flow. Viscous xanthan solutions are opaque, so the colour change can only be detected near the vessel wall. The video clip is divided into separate bmp-images, which were processed by freeware program ImageJ 1.32 (http://rsb.info.nih.gov/ij). The experimental area is selected manually from the pictures and the experimental area is automatically divided into desired amount of rectangular blocks by a java-based routine. The averaged value of green colour (from 0 to 255) is calculated for each block. A relative change of 5 % in any of the blocks initiates the timekeeping. When a block reaches 95% of the equilibrium value the block is considered well mixed [VIII].

2.5 Mass transfer

The volumetric mass transfer rate was investigated by dynamic gassing in – gassing out experiments (van't Riet, 1979). Dissolved oxygen was monitored with a polarographic probe. Usually when calculating the volumetric mass transfer the following assumptions are made: liquid film resistance is dominant, both gas and liquid are ideally mixed, gas concentration and pressure remain constant in the tank. These assumptions make the comparison against CFD or multiblock results rather difficult [VII], since we used CFD and the multiblock to model local conditions and non-ideal mixing. It should be noted that the literature correlations give very different results depending on the used assumptions [IX] (van't Riet, 1979; Middleton, 1992). When dealing with relatively fast mass transfer (>0.05 s^{-1}), the heterogeneous nature begins to affect the calculation of the k_La (Laakkonen, 2006; Middleton, 1992). The volumetric mass transfer coefficient was calculated from dissolved oxygen (DO) measurements, by a natural logarithm of ($c_{DO}{}^{*}-c_{DO}$) was taken and plotted against time. Then the angular coefficient (k_La) of the curve was calculated, the result was normalized to 20 ºC (Jackson and Shen, 1978, eq.1). By using this simple approach we can compare the results to majority of the literature. With the multiblock model the DO concentration curve can be compared against simulations, which is a more fundamental approach than the simplified volumetric mass transfer rate.

$$k_L a_{20} = \frac{k_L a}{1.022^{\theta-20}}$$

(1)

3. MODELLING

For CFD-simulations we used various versions (4/5/10) of a commercial-code CFX. The multiblock model is based on the work of Alopaeus (2002) and Laakkonen (2006). The complex models were implemented trough FORTRAN 77 routines. The multicomponent mass transfer model was linked to an in-house program called Flowbat which has an extensive physical properties database (http://www.tkk.fi/Units/ChemEng/research/Software/flowbat/index.html).

3.1 Levels of modelling

There are significant spatial variations in a stirred vessel that affect reactor performance. Phenomenological models require the local fluid flow information, apparent viscosity and turbulent energy dissipation. CFD is a great tool for calculating detailed fluid flowfields for arbitrary vessel geometries and operating conditions. The downside is that CFD is not suited for calculating long unsteady-state runs. The computational burden also limits the use of CFD in validating the phenomenological sub-models. In this thesis three levels of modelling have been used: the CSTR, a multiblock model and CFD (Figure 7). We calculated flowfields with CFD and validated phenomenological models with the multiblock model. The traditional ideally mixed CSTR was used as a reference case.
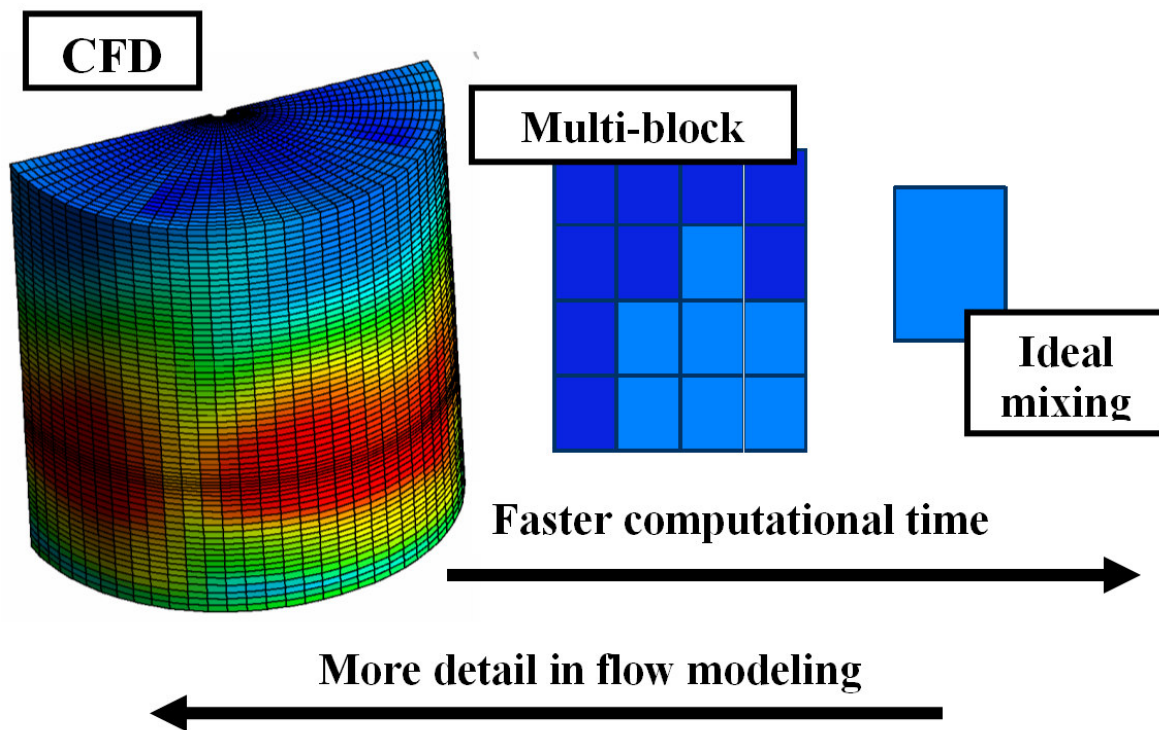
Figure 7. A schematic of different levels of modeling.

Another thing that needs to be considered is the number of sub-models in the reactor-model. In Figure 1 some things that affect gas-liquid mass transfer were presented. It is quite clear that including all of the variables and dependencies into the simulations might make the system too complicated for studying the effects of individual sub-models. The computational cost would be too high if some simplifications weren't made in the simulations. In Figure 8 some of the sub-models are presented.
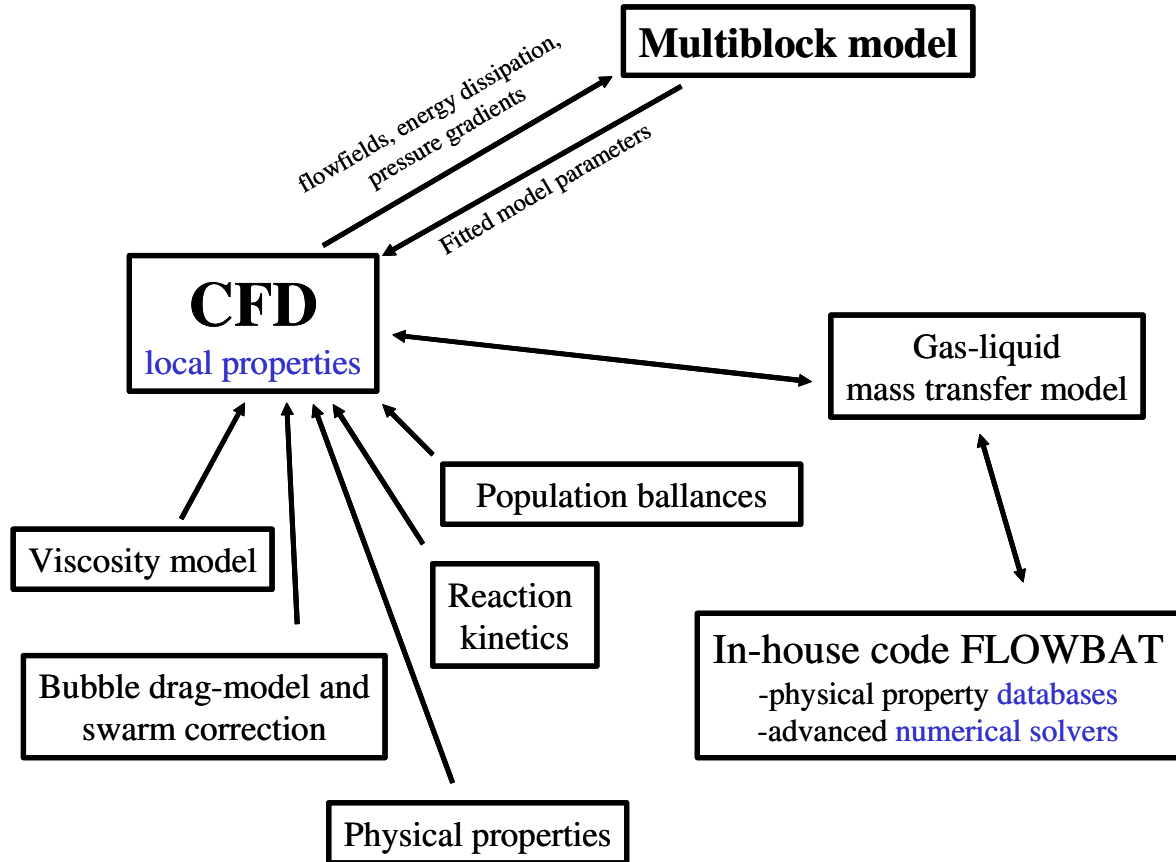
Figure 8. Important user defined sub-model aggregates are presented here.

The inherent complexity of gas-liquid reactors presents a challenge in the model validation. For example the local BSD is a result of the liquid flow field, gas hold-up, turbulence, bubble breakage and coalescence, bubble interaction terms etc. Majority of the models available have been developed for a standard Rushton turbine stirred tanks with a lean air-water system at the fully turbulent flow regime. Unfortunately many industrial reactors operate with non-standard vessel geometries, in the transient turbulence regime with complex non-Newtonian fluids (e.g. bioreactors). There is a need to develop a model that is usable for a wide variety of G-L systems with different physical properties at any scale, vessel geometry and operating conditions.

3.2 The (bio)reaction and its implementation

Reaction kinetics is the underlying reason why G-L flow and mass transfer needs to be modelled. First of all it should be made sure that the reaction kinetics is free of any mass/heat and momentum transfer limitations, if this criteria is not met the simulations will be fundamentally flawed. The primary role of mass transfer and mixing is to supply the reaction with a steady stream of reactants. In mass transfer limited (i.e. slightly soluble gasses) reactors the G-L mass transfer is of the utmost importance to reactor performance. In bioreactors the components produced by bacterial metabolism also need to be removed.

The typical metabolic routes developed by biochemists are too detailed for engineering purposes. For instance: the citric acid cycle is a fundamental metabolic pathway for energy production from carbohydrates, proteins and fats through aerobic respiration (Table 1) and this is just one small part of bacterial metabolism. A detailed model of bacterial metabolism would be computationally extremely demanding and the benefits of using one would be limited when compared against the performance of pseudo component reaction kinetics.

Table 1. The citric acid cycle in ten steps (http://en.wikipedia.org/wiki/Citric_acid_cycle).

	Substrates	Products	Reaction type
1	Oxaloacetate + Acetyl CoA + water	Citrate + CoA-Sh	Aldol condensation
2	Citrate	cis-Aconitate + water	Dehydration
3	cis-Aconitate + water	Isocitrate	Hydration
4	Isocitrate + NAD^+	Oxalosuccinate + NADH + H^+	Oxitation
5	Oxalosuccinate	α-Ketoglutarate + CO_2	Decarboxylaton
6	α-Ketoglutarate + NAD^+ + CoA-SH	Succinyl-CoA + NADH + H^+ + CO_2	Oxitative decarboxylation
7	Succinyl-CoA + GDP + P_i	Succinate + CoA-SH + GTP	Substrate level phosphorylation
8	Succinate + ubiquinone	Fumarate + ubiquinol	Oxidation
9	Fumarate + water	*L*-Malate	Hydration
10	*L*-Malate + NAD^+	Oxaloacetate + NADH + H^+	Oxidation

So, there is a need for simplified bioreaction models that rely on mass balances of pseudo components (e.g. biomass, nutrient, carbon source) for engineering purposes. It's reasonable to view bacteria/fungi/biomass as a small black box reactor that has an input and an output. One example is the xanthan bioreaction (Garcia-Ochoa *et al.*, 1998 & 2000). The reaction is presented in simplified form in equations 2-7 [V]. It is also important to notice that the mass transfer and bioreaction model need to be connected with some key components (see. Fig 9).

$$r_B = 0.535 \cdot c_B \left(0.16466 \cdot c_{B0} + c_{N0}\right) \left(1 - \frac{c_B}{c_{B0} + 6.073 \cdot c_{N0}}\right) \tag{2}$$

$$r_X = 6.0682 \cdot 10^4 \cdot c_{O2} \cdot c_B \left(7.1644 \cdot 10^{-3} + 1344 \cdot c_{O2}\right) \tag{3}$$

$$r_S = -1.1581 \cdot r_X - 985.95 \cdot c_{O2} c_B \left(0.9744 - 4811.6 \cdot c_{O2}\right) - 5.4945 \cdot r_B \tag{4}$$

$$r_{O2} = -3.2496 \cdot 10^{-4} \cdot r_X - 32.865 \cdot c_{O2} \cdot c_B - 7.0413 \cdot 10^{-3} \cdot r_B \tag{5}$$

$$r_N = -0.16466 \cdot r_B \tag{6}$$

$$r_{CO2} = -r_{O2} \tag{7}$$

The downside of including a reaction into the model is the increased computational effort. A typical industrial simulation has ~100000 elements and needs to be run for 1-2 minutes with a timestep of 0.05-0.01s to reach a pseudo steady-state. A comprehensive CFD-simulation of a xanthan bioreaction would include (Figure 9); component balances (12), turbulence balances (2), mass balances (2), momentum balances (6), population balance for bubbles (usually 10-20 groups) and iterative two-film mass transfer, it is imperative to know which things are worth modelling. In short, making long batch simulations with a CFD-model is unfeasible. However with a multiblock model that has been supplied with the flowfield, turbulent energy dissipation and pressure gradients from a 2-phase CFD simulation dynamic batch runs lasting for days can be simulated [V].

	Liquid	Gas
Biomass	X	
Carbon source	X	
Nutrients	X	
Xanthan	X	
O_2	X	X
CO_2	X	X
N_2	X	X
H_2O	X	X
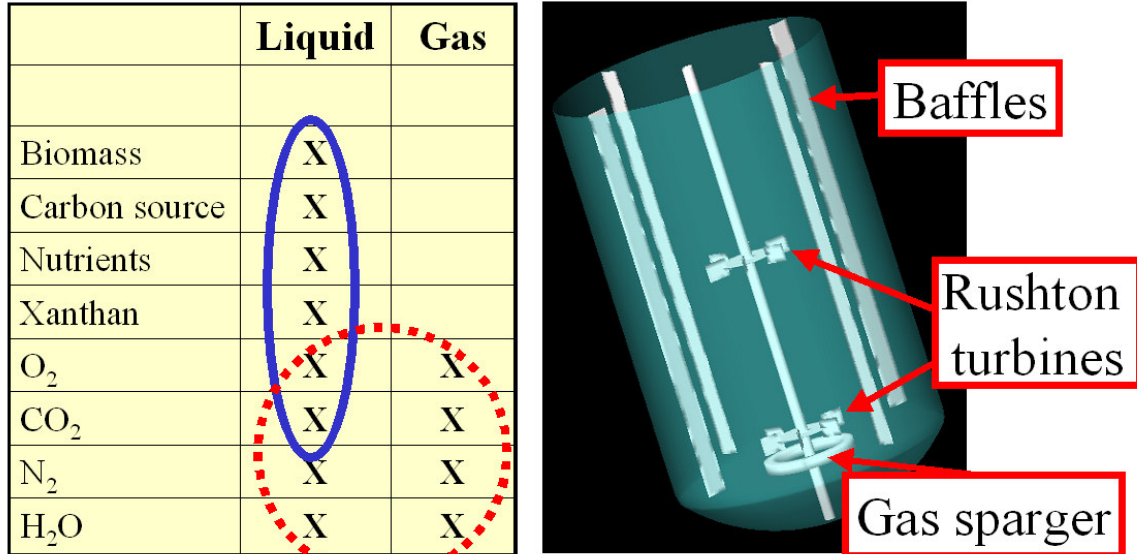
Figure 9. 70 m^3 reactor [IV] and the included component balances. Gas-liquid mass transfer (dashed circle) and liquid phase xanthan bioreaction (continuous circle) interact only trough dissolved oxygen and carbon dioxide (the overlapping area).

3.3 One phase flow field modelling

CFD is based on solving the mass (eq. 8) and momentum (eq. 9) balances. The balances are presented here in a simple vector notation (Bird *et al.*, 1960). On the right hand side are the terms of pressure force, momentum gain by viscous transfer and gravitational force, all are for a given unit volume. In chapters 3.3.1 and 3.3.2 we will take a look how viscosity and eddy viscosity are calculated. If there is no density difference the gravity term becomes negligible in flow modelling, however hydrostatic pressure affects the equilibrium of mass transfer.

$$\frac{\partial \rho}{\partial t} + \nabla(\rho \vec{u}) = 0 \tag{8}$$

$$\frac{\partial(\rho \vec{u})}{\partial t} + \nabla(\rho \vec{u}\vec{u}) = -\nabla p + \mu \nabla^2 \vec{u} + \rho \vec{g} \tag{9}$$

3.3.1 Viscosity model

Typical Newtonian fluids do not need a viscosity model at all since the effects of pressure and temperature are small in ambient conditions. With non-Newtonian fluids viscosity modelling becomes important. In bioreactors viscous shear thinning fluids are common. Carreau (eq. 10) and a Herschel-Bulkley (eq. 11) type viscosity models were used in our work. The Carreau model has an advantage over Casson, Herschel-Bulkley and power law model, because it has a limiting viscosity (μ_0) at zero-shear. If there is no limiter, the viscosity will be infinite at zero shear causing convergence difficulties in CFD simulations.

$$\frac{\mu_{app} - \mu_\infty}{\mu_0 - \mu_\infty} = \left[1 + (\lambda \gamma_{tot})^2\right]^{(n-1)/2} \tag{10}$$

$$\mu_{app} = \frac{\tau_0 + K \cdot \gamma_{tot}{}^n}{\gamma_{tot}} \tag{11}$$

Herschel-Bulkley viscosity model parameters were fitted based on measurements from 0…4 wt-% xanthan (Keltrol BT) solutions. The model is presented in equations 12-15, the Herschel-Bulkley accounts for the yield-stress that is apparent in many shear thinning fluids. It is notable that the value of n has a minimum at 0.9 wt-% xanthan. It is noted here out that sub-models that only use n to describe effect of viscosity, could give unreasonable results because of oversimplification. All other viscosity model parameters increase with increasing xanthan concentration. A minimum shear rate of 0.1 s^{-1} was set to avoid convergence difficulties.

$$K = 22.0 \cdot (1 - e^{0.016387 \cdot \frac{c_x}{wt-\%} - 0.607352 \cdot \frac{c_x}{wt-\%}{}^2}), \frac{c_x}{wt-\%} \geq 0.027 \tag{12}$$

$$K = 0.001, \frac{c_x}{wt-\%} < 0.027 \tag{13}$$

$$n = e^{(-3.9248 \cdot \frac{c_x}{wt-\%})} + 0.3421 \cdot (1 - e^{\frac{-c_x}{wt-\%}/1.8553}) \tag{14}$$

$$\tau_0 = 1.382 \cdot \frac{c_x}{wt-\%}{}^{1.483} \tag{15}$$

3.3.2 Turbulence modelling

Even though turbulence is one of the millennium price problems and worth one million dollars if solved (http://www.claymath.org/millennium/), for low viscosity Newtonian liquids there are a number of efficient turbulence modelling approaches: RANS (Reynolds Averaged Navier Stokes), RSM (Reynolds Stress Model), LES (Large Eddy Simulation) and DNS (Direct Numerical Simulation). Turbulence modelling is a separate field of science and there are loads of studies on Newtonian fluids in the turbulent regime. Majority of the work has done on simple geometries and fully turbulent flow, which is a limitation. Here, the focus is on viscous fluids and transitional turbulence regime ($10 < Re_{imp} < 10000$) to find out which RANS models are suitable for modelling fermenters.

$$Re_{imp} = \frac{D_{imp}^2 N \rho}{\mu_{app}} \tag{16}$$

Turbulence modelling is closely tied to the viscosity model. The flowfields are calculated based on the sum (eq. 17) of the apparent viscosity and eddy viscosity (eq. 18, standard k-ε model). If either of the terms is an order of magnitude smaller than the other its influence is minute and accurate modelling of it is not that important for the simulation. Often, phenomenological sub-models require the local turbulent energy dissipation (Figure 2). The simulated total turbulent energy dissipation was linearly scaled according to measured power consumption in order to reduce model related inaccuracies. The dissipation then equals the mechanical energy input. The scaled turbulent energy dissipation is only used in the user defined models, not in the flow calculations.

$$\mu_{tot} = \mu_{app} + \mu_{eddy} \tag{17}$$

$$\mu_{eddy} = \rho C_\mu \frac{k^2}{\varepsilon} \tag{18}$$

3.4 Two phase flow field modelling

Two-phase flow was modelled with the Eulerian-Eulerian approach, where the phases are assumed to be interpenetrating continua. One of the phases is defined as continuous (k=1) and the other as dispersed (k=2), the phases sum up to unity. The pressure and gravity vectors are shared by both phases, whereas the other variables are phase specific. The only notable change to the one phase solution is the presence of interfacial forces M_{if}. Fortunately, in mechanically agitated vessels the drag force is dominant over other phase interaction terms and the other interfacial forces can be discarded for the sake of simplicity (Tabib et al. 2007; Wachem and Almstedt 2003). Implementation of the important interfacial forces (M_{if}) is discussed in chapter 4.2.1.

$$\frac{\partial(\alpha_k \rho_k)}{\partial t} + \nabla(\alpha_k \rho_k \vec{u}_k) = 0 \tag{19}$$

$$\frac{\partial(\alpha_k \rho_k \vec{u}_k)}{\partial t} + \nabla(\alpha_k \rho_k \vec{u}_k \vec{u}_k) = -\alpha_k \nabla p + \alpha_k \mu_k \nabla^2 \vec{u} + \alpha_k \rho_k \vec{g} + \vec{M}_{if} \tag{20}$$

$$M_{if} = M_{drag} + M_{mass} + M_{lift} + M_{disp} + ... \tag{21}$$

3.4.1 Population balances for bubbles

A realistic local bubble size distribution is the key factor in successful modelling of G-L interactions and mass transfer rate. Population balance for bubbles with breakage and coalescence has already been discussed by Laakkonen 2006 in great detail. First we developed a model for low viscosity fluids, based on air – water and CO_2 – butanol dispersions [III, VI]. Then we started looking for a model/parameter combination which could cover a wider range of physical properties and operating conditions. The commercial CFX-software has a built-in multiple size group model (MUSIG) (Lo, 2000) that allows modification of the coalescence and breakage models. The method uses several discrete bubble classes and calculates the dispersed phase slip-velocity based on the local Sauter mean diameter (d_{32}). Bubble breakage and coalescence models are needed to close the PB equation, the growth term was considered to be minute and it was left out of the simulations.

Population balance for bubbles =

Transportation in/out balance region +
Birth/death by breaking +
Birth/death by coalescing +
Growth/size reduction by mass transfer or pressure

The selected models are: bubble breakage rate model of Luo and Svendsen (1996) with daughter bubble size of Lehr et al. (2002) Bubble coalescence of Coulaloglou and Talvarides (1977) and coalescence efficiency of Chesters (1991). This combination proved to be usable for both air - water and viscous air – xanthan dispersions [V, VIII, IX]. Experimentally determined values in equations (10)-(13) are $C_1 = 0.14$, $C_2 = 0.3$, $C_3 = 0.88$, $C_4 = 0.6$. The parameter fitting was done based on experiments from the 0.2 m^3 Rushton agitated vessel in the xanthan concentration range of 0 - 0.75 wt-%. The details are given in Laakkonen (2006) and [V]. With increased vessel hold-up it becomes more and more difficult to make representative measurements. It is not reasonable to fit coalescence model parameters to data from lean dispersions where the phenomenon is not controlling.

$$g(d_k) = C_1 \cdot (1-\alpha)\left(\frac{\varepsilon}{d_k^2}\right)^{1/3} \int_0^1 \int_{\xi_{min}}^1 \frac{(1+\xi)^2}{\xi^{11/3}} \exp\left(-\frac{6 \cdot \sigma \left[f^{2/3} + (1-f)^{2/3} - 1\right]}{\rho_C \varepsilon^{2/3} d_k^{5/3} \xi^{11/3}}\right) d\xi \, df \tag{22}$$

$$\beta(d_n, d_p) = \begin{cases} \dfrac{6}{\pi^{3/2} d_n^3} \dfrac{\exp\left(-9/4 \cdot C_2 \left[\ln\left(2^{2/5} d_n \varepsilon^{2/5} (\rho_C/\sigma)^{3/5}\right)\right]^2\right)}{1 + erf\left(3/2 \cdot \ln\left[2^{1/15} d_p \varepsilon^{2/5} (\rho_C/\sigma)^{3/5}\right]\right)}, & 0 \le d_n^3 \le \dfrac{d_p^3}{2} \\[4mm] \beta(d_p - d_n, d_p), & \dfrac{d_p^3}{2} \le d_n^3 \le d_p^3 \end{cases} \tag{23}$$

$$h(d_k, d_p) = C_3 \cdot \varepsilon^{1/3} (d_k + d_p)^2 (d_k^{2/3} + d_p^{2/3})^{1/2} \lambda(d_k, d_p) \tag{24}$$

$$\lambda(d_k, d_p) = \exp\left(-C_4 \sqrt{\frac{We}{2}}\right), \tag{25}$$

$$We = \frac{\rho_C d^{5/3} \varepsilon^{2/3}}{\sigma} \tag{26}$$

Discretisation is an important practical issue in modelling PB's with CFD. Is typical simulation it is desirable to set the number of bubble-classes as low as possible, because solving population balances are computationally time consuming. When using a limited number of classes the discretisation of the classes becomes increasingly important. If the number of classes is too low, the simulation will likely crash due to high coalescence and breakage rates. We found out that the built-in discretisations in CFX were not suitable for our needs. Thus, a simple geometric discretion was created (eq. 27-28). This approach generates a dense discretisation with smaller bubbles, where most of the mass transfer area is located and a looser one for the large bubbles which hold the majority of reactor gas-volume. It is emphasized that the discretisation must be adapted case by case, since the differences in the range of a local BSD ranges from 0...3 mm with CO_2-butanol to 0...50mm with viscous xanthan solutions.

$$d(i) = d_{min} \cdot G^i \tag{27}$$

$$\Delta d = \frac{\left(d_{min} \cdot G^{i+1}\right) - \left(d_{min} \cdot G^{i-1}\right)}{2}, \tag{28}$$

For comparison, a simpler PB approach (Wu *et al.*, 1998; Kerdouss *et al.*, 2006, Lane *et al.*, 2005; Lane, 2006) of bubble number density (BND) was included in the CFD simulations [IX] (eq. 23-29). The BND approach only requires the modelling of a single scalar with coalescence and breakage functions. MUSIG model uses N bubble classes with the breakage/coalescence matrices of size $N \cdot N$. A two-phase BND simulation required roughly 50% of the computational time that is needed to calculate a similar 10 group MUSIG-simulation, note that the turbulent base case gas-liquid simulation requires 10 balances to be solved. The parameter values are We_{CR} = 1.5, C_{CO} = 0.05, and C_{BR} = 0.075. The BND model was used to model an air-water system [IX] and compared against MUSIG-results.

$$\frac{\partial n}{\partial t} = S_{BR}n - S_{CO}n^2 \tag{29}$$

$$n = \frac{\alpha}{(\pi/6)d^3} \tag{30}$$

$$S_{BR} = C_{BR}(1-\alpha)\left(\frac{\varepsilon}{d^2}\right)^{1/3}\exp\left(\frac{We_{CR}}{We}\right), We > We_{CR} \tag{31}$$

$$S_{BR} = 0, We < We_{CR} \tag{32}$$

$$S_{CO} = C_{CO} \cdot (1-\alpha) \cdot \eta_{CO}\varepsilon^{1/3}d^{7/3}, \tag{33}$$

where

$$We = \frac{\rho_C d^{5/3}\varepsilon^{2/3}}{\sigma} \tag{34}$$

$$\eta_{CO} = \exp\left(-\sqrt{\frac{We}{8}}\right) \tag{35}$$

3.4.2 Gas-liquid interactions

In order to verify G-L interaction models the local bubble size, gas hold-up and liquid flow field need to be reasonable. An exact verification of the models is difficult, since there are several counteracting phenomena. It is known that turbulence affects gas flow by increasing turbulent viscosity (eq. 36) (Bakker and van den Akker, 1994). Turbulent dampening of slip velocity decreases the slip velocity of bubbles. A suitable value for C_5 is 0.06 [VI], in typical stirred tanks the turbulent increase on apparent bubble viscosity is < 0.1 Pa·s. Thus, turbulent dampening of slip-velocity is only significant when working with low viscosity fluids (e.g. Air-Water).

$$\mu_{bub} = \mu_{app} + C_5\rho_C\varepsilon^{1/3}d_{32}^{4/3} \tag{36}$$

The accurate modelling of bubble rise (slip/terminal) velocities is important, since they affect the gas hold-up and hence the mass transfer area between gas and liquid. The bubble slip velocity (U_{slip}) is solved from equation (37). It is a force balance between buoyancy, pressure gradient and the opposing friction between the bubble and liquid.

$$[(\rho_C - \rho_D)\vec{g} + \nabla p]V_{bub} = 0.5 \cdot C_D A_h \rho_C \vec{U}_{slip}|\vec{U}_{slip}| \tag{37}$$

There are many ways to calculate the drag coefficient (Chhabra 2007; Clift *et al.*, 2005), but the drag coefficient is really not that critical. This is due to the MUSIG-model, which uses the average local bubble size (usually over 1 mm), resulting in minute differences in the drag coefficient. The accurate prediction of the bubble size is much more important when calculating the bubble slip-velocity, since the buoyancy force is proportional to d^3 and the drag coefficient is only a multiplier. Recently, I have favoured drag models by Tsournakos *et al.* (2004; eq. 38) or Margaritis *et al.* (1999) with a bubble shape correlation (Miyahara *et al.*, 1993; eq. 40) that accounts for the non-sphericity of bubbles in non-Newtonian liquids. The bubble shape correlation affects bubble drag via the used bubble diameter (the *d* used in drag calculations is *E(d)·d(spherical bubble)*).

$$C_D = \begin{cases} \dfrac{24}{Re}\left(1 + 0.173\,Re^{0.657}\right), Re < 135 \\ 0.95, Re > 135 \end{cases} \tag{38}$$

$$Re = \frac{d_{32} \cdot U_{slip}\rho_c}{\mu_{bub}} \tag{39}$$

$$E(d) = \begin{cases} 1.1, & Re \cdot Mo^{0.078} < 4 \\ 1.88 \cdot \left(Re \cdot Mo^{0.078}\right)^{-0.386}, & 4 \le Re \cdot Mo^{0.078} \le 15 \\ 0.66, & 15 < Re \cdot Mo^{0.078} \end{cases} \tag{40}$$

$$Mo = \frac{g \cdot \mu_{app}^{4}}{\rho_C \cdot \sigma^3} \tag{41}$$

When modelling viscous fluids the interactions between bubbles or the time dependent effect on the viscous media becomes increasingly important. Some articles have investigated G-L interaction and its effect on the bubble slip velocity (Li, 1999; Chhabra, 1998). But these described effects were found to be too low when compared against experiments [IV]. We investigated a stream of bubbles rising in a stagnant fluid [IV] and found out that the bubble swarm effect makes a huge difference (Figure 10, eq. 42). The bubble swarm correction increases the bubble rise velocity significantly, by decreasing the apparent viscosity by increased shear in pseudoplastic fluids. An interesting observation was that the bubbles tended to form trails of several bubbles [V] (Figure 11). The derivation and the implications of equation 42 are explained in publication IV.

$$\gamma_{tot} = \gamma_{liq} + \frac{U_{slip}}{d}\left(1 + K\frac{\alpha^{(1/3)}}{1-\alpha^{(1/3)}}\right) \qquad (42)$$
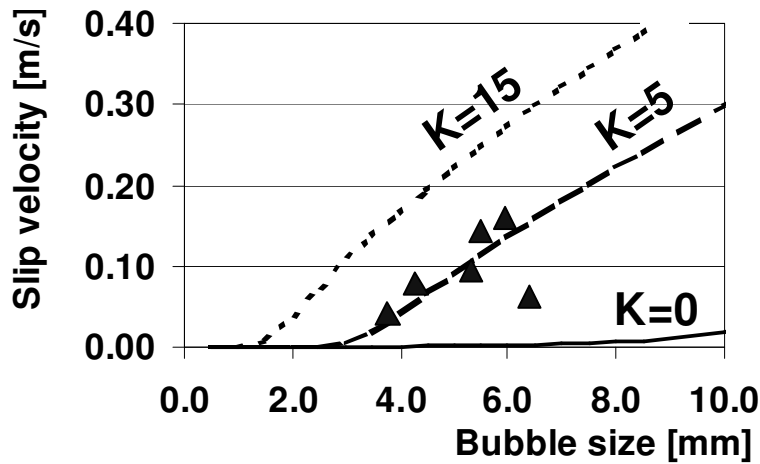
Figure 10. Experimental [▲] and calculated slip-velocities vs. bubble size with varying bubble swarm correction (*K*) values. 0.75 w-% xanthan solution, gas volume fraction = 0.05, 1D-calculation. [IV]
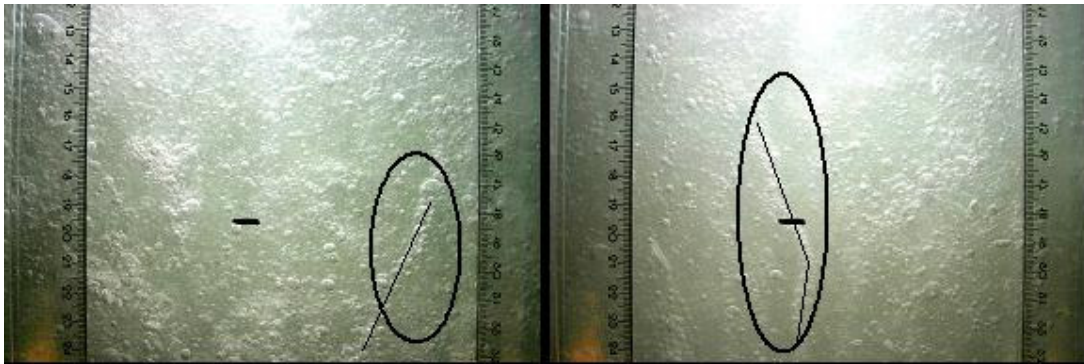
Figure 11. Bubble trails in 0.25 wt-% xanthan solution. 200 dm^3 vessel, 0.5 vvm, 390 rpm, RT, impeller plane.

Without the swarm correction gas accumulated in the vessel and the results became physically unreasonable (very high gas hold-up) in the single bubble size simulations [IV]. The accurate modelling of bubble rise velocities is important, since they affect the gas hold-up and hence the mass transfer area between gas and liquid.

3.4.3 Gas-liquid mass transfer modelling

Gas-liquid mass transfer is limited by vapour-liquid equilibrium. There is an equilibrium value of the dissolved gas (C_L^*) that depends on pressure, temperature and phase composition. This value can be measured experimentally [I] for binary-pairs or estimated from various correlations, which can be used to describe multicomponent systems. An accurate prediction of VLE is equally important than predicting a correct $k_L a$ in mass transfer limited systems, since the equilibrium concentration (C_L^*) affects the mass transfer flux (eq. 43)

In literature most of the mass transfer experiments are described in the form of k_La. The traditional way to model vessel averaged G-L mass transfer is presented in (eq. 43), a more fundamental approach is to think as (eq. 44). The traditional approach is usually based on semi-empirical k_La correlations, which lump a lot of phenomena into a single package and assume ideal mixing. These correlations are usually reliable when used to describe similar systems (same geometry, scale, operating conditions and components on which they were fitted. Often the system is assumed to be ideally mixed, which is not the case with G-L stirred vessels [VII, VIII].

$$\text{RATE} = k_La \cdot (C_L^* - C_L) \tag{43}$$

$$\text{RATE} = \int (\text{local FLUX} * \text{local G-L AREA}) \, dV \tag{44}$$

The flux term (eq. 44) is a product of mass transfer resistances and the driving force. The gas-liquid area term is formed from gas hold-up and the characteristic mass transfer area, which is calculated from the BSD. A simplified way to model the mass transfer rate is to model the local k_La separately as described in equation 45. The mass transfer resistance in liquid film (k_L) (Kawase *et al.*, 1992; eq. 40) is based on the penetration theory of Higbie, developed for single bubble in an isotropic turbulence field, the used value of parameter C_6 is 0.3 [V].

$$k_La = k_L \cdot a \tag{45}$$

$$k_L = C_6 \sqrt{D_L} \left(\frac{\varepsilon \cdot \rho_C}{\mu_C} \right)^{1/4} \tag{46}$$

4. RESULTS AND DISCUSSION

4.1 Experimental

### 4.1.1 Bubble size distributions

The presented BSDs are subject to many simplifications. Bubbles are not of the same size and spherical as so often assumed (Figure 12), surface tension, turbulence, liquid flow and apparent viscosity have a significant effect on the local BSD. All methods have their advantages and downfalls; none of the current experimental methods covers the whole spectrum of bubble sizes, experimental conditions or chemical systems. The accurate measurement of local bubble sizes is notoriously difficult (Alves *et al.*, 2002).
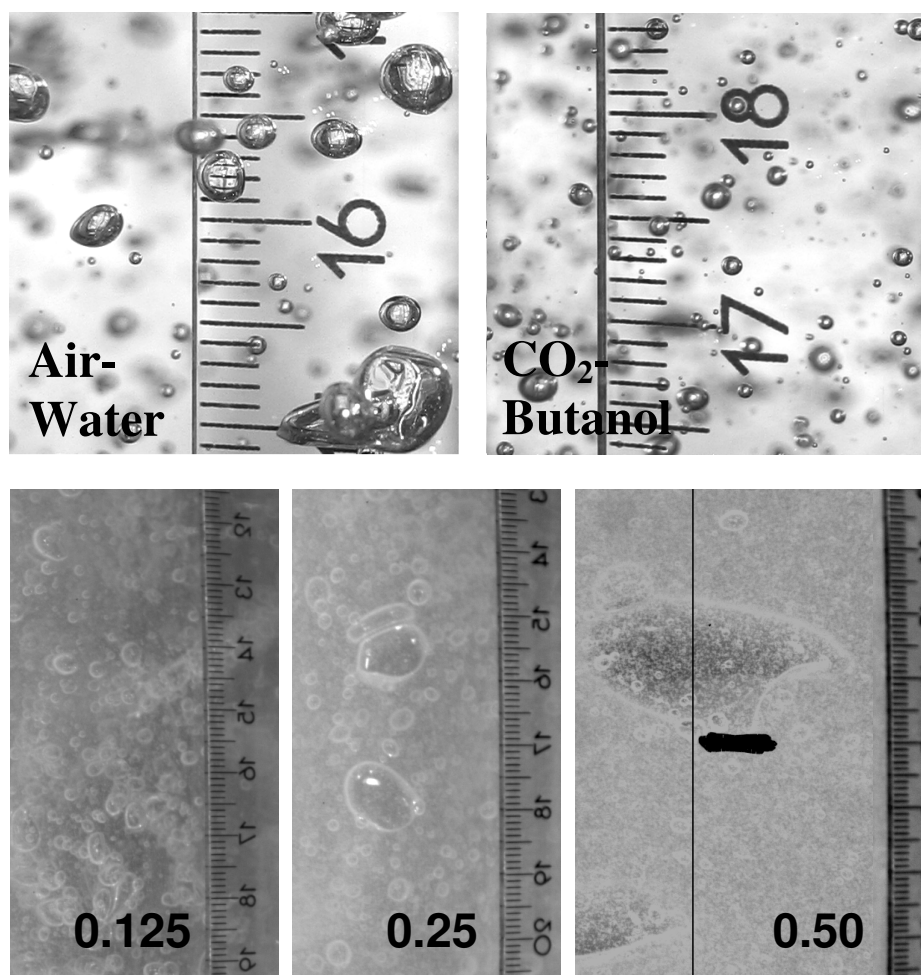
Figure 12. Variation is local bubble sizes, visualized by photography. CO_2-butanol and air-water (14 dm^3 vessel, RT, 0.07 vvm, 340 rpm) Air-aqueous xanthan solutions 0.125, 0.25 and 0.50 wt-% (200 dm^3 vessel, RT, 0.5 vvm, 390 rpm). Scale is in centimetres.

Digital photography: There are two ways to analyse the photographs; automatically or manually, both need huge amounts of bubbles to be identified in case of wide BSDs. Manual analysing is very laborious, but the results are more accurate than the results from an automated analysis. Manual identification can be performed on relatively dense dispersions (~10 vol-%). The advantage of the automated picture analysis is that it can quickly analyse large amounts of

measurement data, but this method is more prone to errors (Figure 13) when dealing with overlapping bubbles (A), bubbles with light reflection (B) or very small bubbles (C). Because the method has limitations with overlapping bubbles it can only be reliably used with lean dispersions (<1 vol-%). The major advantage of photography is that it can be used to measure almost any bubble size with appropriate optics and the method can cover a wide range of bubble sizes.
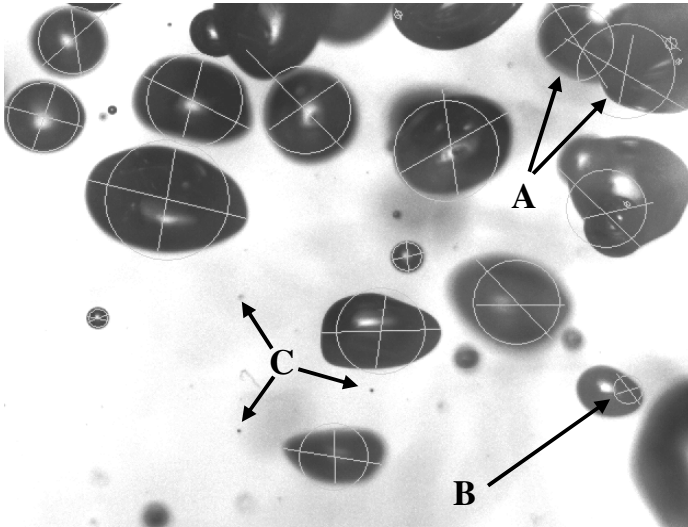
Figure 13. Uncertainties in automated image analysis.

Presentation of the results: There is a need to compare different experimental methods and simulations. So, post-processing the results plays an important part in analysing them. The comparison is possible by defining the BSDs in dimensionless form. The number densities are defined as

$$n(d_i) = \frac{d_{max} - d_{min}}{\Delta d_i} \frac{N_i}{\sum\limits_{j=1}^{NC} N_j} \tag{47}$$

and volumetric densities as

$$v(d_i) = \frac{d_{max} - d_{min}}{\Delta d_i} \frac{N_i d_i^3}{\sum\limits_{j=1}^{NC} N_j d_j^3} \tag{48}$$

There are alternative ways to present the results and compare experiments against simulations. In article [IX] the CSP is used as an experimental technique to investigate local BSDs. However the measurement range of the apparatus is rather limited when compared against CFD simulations. A reasonable approach is to investigate the local BSD in the CSP measurement range (1.0-6.2 mm) by scaling results to fit $\sum\limits_{i=1} v(d_i) \cdot \Delta d_i = 1$. This approach allows investigating the change in the shape of BSDs in greater resolution, because it is focused on the experimental BSD range. An example of the difficulty of comparing CSP measurements against CFD simulations is presented in Figure 14. The number density peak is below the CSP detection range and drawing

conclusions between measurements and simulations makes no sense. However, the experimental volumetric distributions can be compared against the CFD simulations to gain new insight if the limited CSP detection range is taken into account.
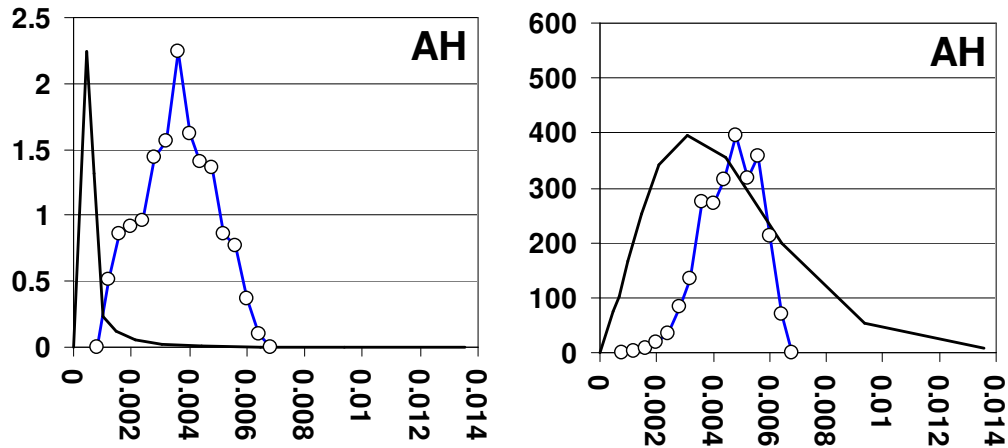
Figure 14. Comparing CSP measurements (dots and line) against simulations (continuous line) [IX]. The BSD's are scaled to have the same peak height. Number density distribution (left), volumetric density distribution (right).

It is important to understand what system we are dealing with and how well the measurement technique is able capture its main characteristics (Figure 15). We need to know which quantities to measure and know if the measurement technique can cover the whole range of bubble sizes. For instance, in lean air-water dispersion there are very small bubbles present (PDA, trend of DI), but the majority of the gas is in the larger bubbles (DI, CSP). When dealing with mass transfer modelling the volumetric BSD and Sauter mean diameter (d_{32}) are the most used, since they describe the relative mass transfer area in respect of the total gas volume. In Table 2 the experimental methods for BSD determination are compared. All the methods have severe limitations with industrial fluids and operating conditions, which include dense/opaque/particulate/corroding dispersions, high gassing rates and intense mixing.
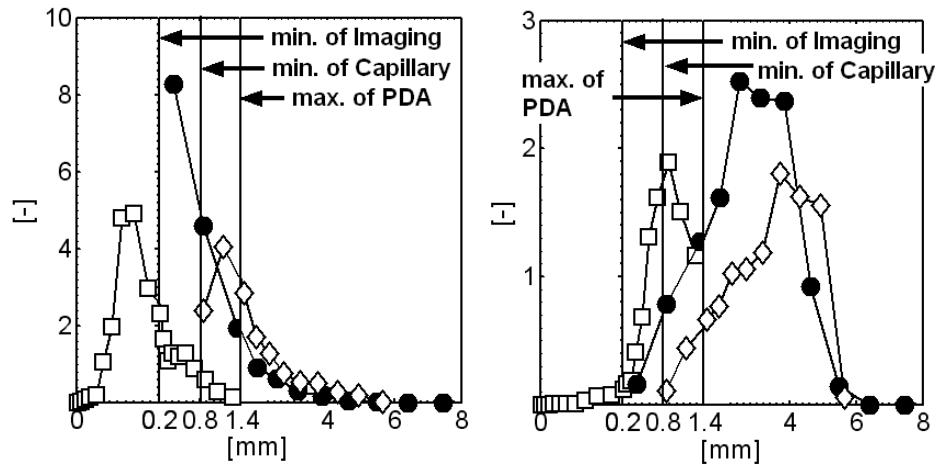
Figure 15. Number (left) and volumetric (right) bubble size distributions of air-water system in the 13.8 dm³ vessel, stirring speed 490 rpm, location A of the stirred vessel [II], —□— phase Doppler anemometry —●— digital imaging, —◇— and capillary technique.

Table 2. Comparison of experimental BSD techniques

Experimental method	Range of applicability	Local gas hold-up	Physical requirements	General notes
Capillary Suction Probe (CSP)	0.4 – 8.0 mm	< 25 %	Low viscosity dispersion. No solid particles allowed.	Invasive method. May disturb flow pattern. Isokinetic sampling is needed.
Phase Doppler Anemometry (PDA)	30 µm-1.4 mm	< 5 %	Transparent dispersion.	Limited to small and spherical bubbles.
Photography with automated image analysis	1 µm - depends on optics and equipment	< 1%	Transparent dispersion.	Identification algorithms need improvement, depth of focus (DOF) correction needed
Photography with manual image analysis	1 µm - depends on optics and equipment	< 10 %	Transparent dispersion.	Manual identification of bubbles is laborious, depth of focus (DOF) correction needed, limited to vessel walls in dense dispersions

4.1.2 Viscous gas-liquid behaviour

In our experiments viscous xanthan solutions exhibited interesting dynamic behaviour. The gas hold-up rises steadily with agitation until it reaches a certain level [IV]. It seems that this level is relatively independent of the xanthan concentration, but stabilization takes longer to achieve with increasing concentration. After the agitation has been stopped, there remains a residual gas hold-up. The residual hold-up is composed of very small bubbles (Venneker, 1999) that are not able to escape from the fluid. This behaviour is suggested (Machon *et al.*, 1980) to be a result of a pseudoplastic behaviour rather than high viscosity. The bubbles can be partially removed by briefly agitating the vessel which promotes bubble coalescence and thus increases the bubble slip velocity. It is probable that these trapped bubbles do not affect the mass transfer rate. The mass transfer area is large, volume of the bubbles small and the residence time is long, so the bubbles are most likely at equilibrium. A related effect is the bubble train effect, the slip-velocity of a bubble increases if it follows the wake of a previous bubble: these bubble trains can be seen in (Figure 11) and in the slip velocity measurements. It is difficult to include these phenomena into CFD-simulations. The gas hold-up accumulation takes too much time to be simulated and both the MUSIG and BND models use a common local bubble size for all bubbles in the computational element. This means that the rise velocity for large and small bubbles is the same and effectively eliminates the possibility of small bubble accumulation. To accurately set a bubble train G-L interaction term we should be sure that our turbulent dampening of slip-velocity and local BSD are correct. The bubble swarm correction was used in article [IV].

4.2 Basic flow modelling

4.2.1 Viscosity models

Many viscosity models were investigated (Power law, Casson, Carreau, and Herschel-Bulkley). The selection of a viscosity model can't be considered to be a critical factor in non-Newtonian gas-liquid modelling as all the investigated models produced nearly identical results. It is suggested to avoid vessels averaged viscosity modelling approaches like Otto-Metzner, which include experimental vessel geometry dependent parameters (*A*) (eq. 49). Another thing to avoid is the infinite viscosity resulting from zero shear. This can be avoided by using models that have a viscosity cap (eq. 10) or by using a minimum shear rate.

$$\mu_{app} = K \cdot \left[A \cdot N \right]^{n-1}$$
(49)

4.2.2 Turbulence models

In this work it was observed that some turbulence models can create unrealistic (Figure 17) eddy viscosities in stagnant areas (transitional or laminar turbulence regime) of the vessel. The eddy viscosity needs to be continuously monitored to see if the results are realistic. The impeller Reynolds number is generally accepted to describe turbulent conditions of a vessel (eq. 14). The assumptions are that a flow with <10 is laminar and >10000 is turbulent. The downfall of this approach is that the reactor is often treated as ideally mixed. For example the widely documented cavern formation contradicts this approach.

It was observed that standard k-epsilon turbulence model does not work well in the transitional turbulent regime. It is likely that the dissipation, convection or the generation of turbulent energy

is mispredicted. It was found out that the shear stress transport (SST) and k-Ω turbulence models predicted reasonable eddy viscosities even in viscous solutions with the RT. When CJ and PJ were modelled, all common turbulence models predicted unreasonable turbulent viscosities [IX] (Figure 17). If a highest turbulent eddy viscosity is not located in the impeller discharge, the turbulence modelling is not working as it should. In areas of low Reynolds number the contribution of dissipation from average flow velocity could have improved the accuracy of predicting the total energy dissipation in the vessel.
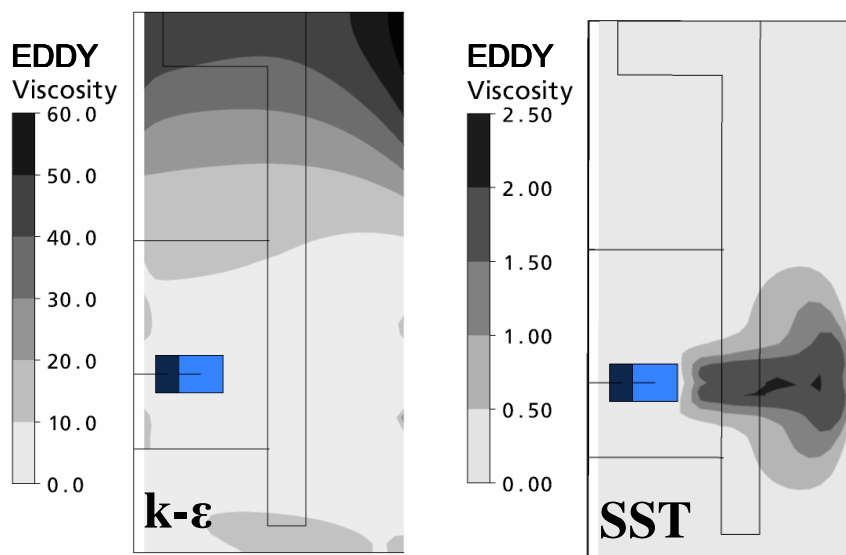
Figure 17. Eddy viscosities [Pas] predicted by k-ε and SST turbulence models. RT, 200dm^3, 0.75 wt-% xanthan, 390 rpm, Note the different scale.

4.2.3 Grid resolution

It is known that CFD has a tendency to under predict turbulent energy dissipation and that increasing the number of computational nodes improves the accuracy of simulations [VII]. In several articles [VII, VIII] grid density and its effect on the accuracy on the simulations was discussed. It was found out that the flowfields are predicted fairly accurately, even with coarse (~60k nodes) grids. The effect of grid resolution is smaller than the effect of the sub-models. The reactor dead-space was not significantly affected by grid resolution when modelling cavern formation with a shear thinning fluid [VIII]. Effects of under predicted turbulent energy dissipation can be corrected by scaling against the experimental value, but this does not affect the flow just the used sub-models. If the grid is kept constant we can investigate complex sub-models with reasonable simulation times. Based on these results it seems that grid resolution is not a critical issue in G-L reactor modelling. Reasonable results can be obtained with fairly coarse computational grids.

4.2.4 Transient or steady-state?

There are two common ways to model impeller motion. First, the multiple frames of reference (MFOR) where the impeller is fixed into one position in respect of the baffles. Second, a more fundamental way is to gradually rotate the impeller in the computational domain and make a time dependent simulation. The latter approach is much more time consuming, than the steady-state MFOR approach. Difference in simulation results between these approaches in standard

mixing vessels is minute [IX]. The transient effect is larger when impeller diameter is increased or the number of blades is reduced. The CJ was the only impeller in which the transient simulation produced a notable (>1 %) difference in simulated k_La. It is acknowledged that in reality bioreactors exhibit time-dependent behaviour, such as the increase in gas hold-up with time and the gathering of gas-slugs which result in time-dependent fluctuations in gas hold-up [IV, VIII]. Although, these phenomena are interesting, a satisfactory result can be obtained by making a steady-state simulation.

4.2.5 Local mixing time simulations

Mixing time simulations are difficult for averaged RANS models (Hartmann, 2005). Recent LES simulations have shown that neglecting the inherently transient nature of turbulence significantly increases mixing times due to the lack of turbulent dispersion (Hartmann *et al.*, 2006). There are turbulent dispersion models available for RANS models but they fail to notably affect the mixing times, so they were not used in this work. By comparing simulation results against local mixing time experiments the combined effect of the used viscosity model and turbulence model can be evaluated. A new approach for analysing local mixing times was developed (Visuri *et al.*, 2007). In our simulations there was a dead-space at the surface of the vessel [VIII] that was not seen in the experiments resulting in erroneous local mixing times, but in the cavern area the local mixing times were at odds. The difficulties in modelling local mixing times accurately may result from the following: modelling the impeller as a thin stationary wall, under prediction of the flow number, turbulence model failure at the transitional flow regime or the viscosity model fails to describe rheology of the fluid in required detail (Yaseen *et al.*, 2005) Apparently steady state RANS approach is not accurate enough to describe local mixing times, resolving the turbulent structures with LES would be a better choice.

4.2.6 PIV measurements vs. CFD simulations

Some work has been previously done with PIV to measure dilute shear thinning fluids (Venneker, 1999). Measurements in viscous fluids are difficult due to small bubbles entrapped in the liquid (Figure 18). This is illustrated in Figure 20b where with increasing xanthan concentration the experimental results deteriorate, there are more errors in the measurements and there is more fluctuation in the results. Here, previously unpublished PIV measurements are presented to verify one phase CFD-simulations (Figure 19). There is a qualitative agreement between the simulations and experiments, although the absolute values differ. The CFD simulations were able to capture cavern formation with 0.4 wt-% xanthan solution and the change of the flow field from radial to axial with the CJ-impeller at low stirring speed (Figure 19, 20ab) [IX]. The CFD-simulations are snapshots taken from a single plane whereas the PIV-results are averaged over 50 sets of snapshot flowfields. These findings support the assumption that CFD is able to predict one-phase flowfields with reasonable accuracy.
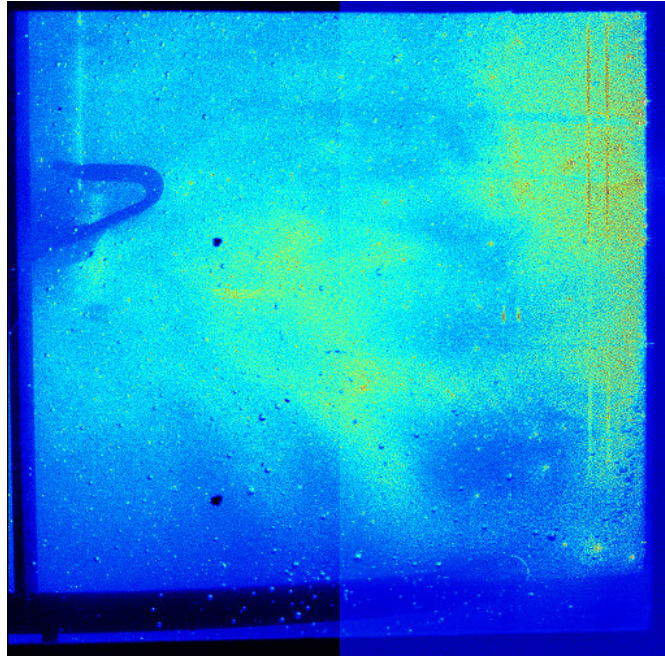
Figure 18. PIV raw data picture of 0.4 wt-% xanthan solution agitated by a CJ, there are tiny entrapped bubbles that interfere with the measurement (showing in green).
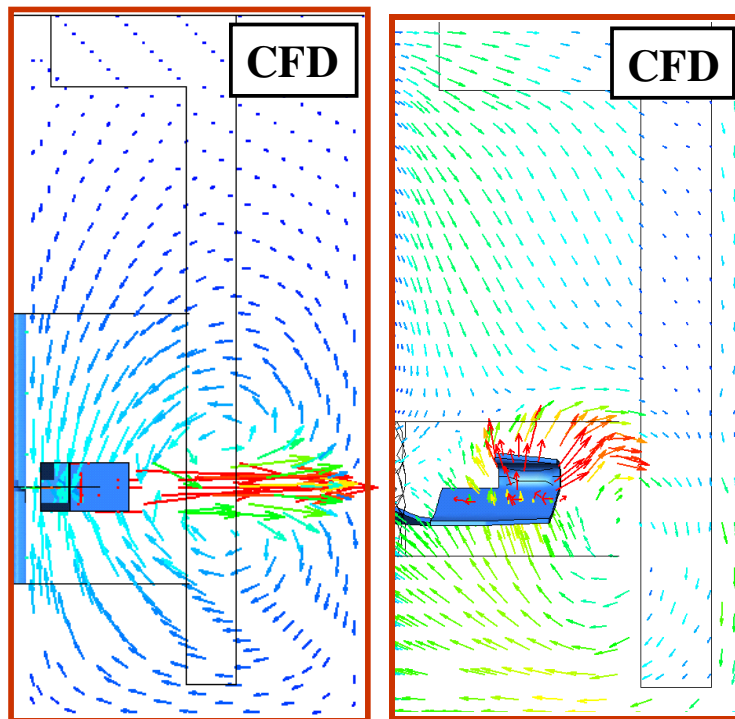
Figure 19. One phase CFD simulations of 0.4 wt-% xanthan solution (left) and water simulation with CJ (right), impeller tip speed 1.35 m/s, the vectors are scaled to match the PIV experiments in Figures 20ab.
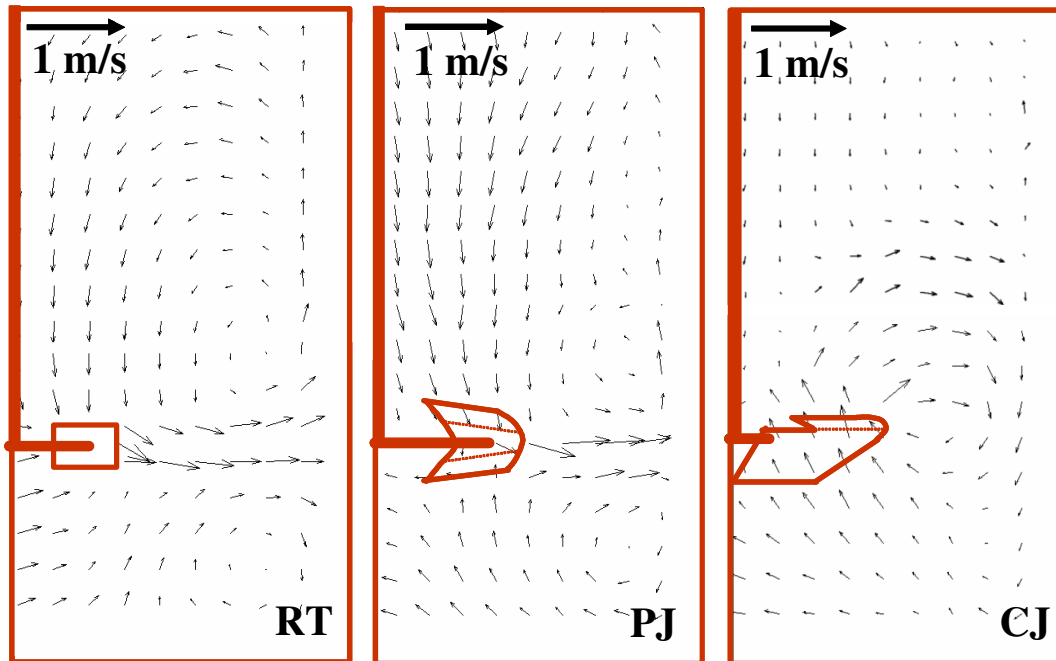
Figure 20a. PIV-results with three different impellers, 14 dm^3 vessel, water, impeller tip speed 1.35 m/s. The CJ corresponds with CFD-simulation in Figure 19.
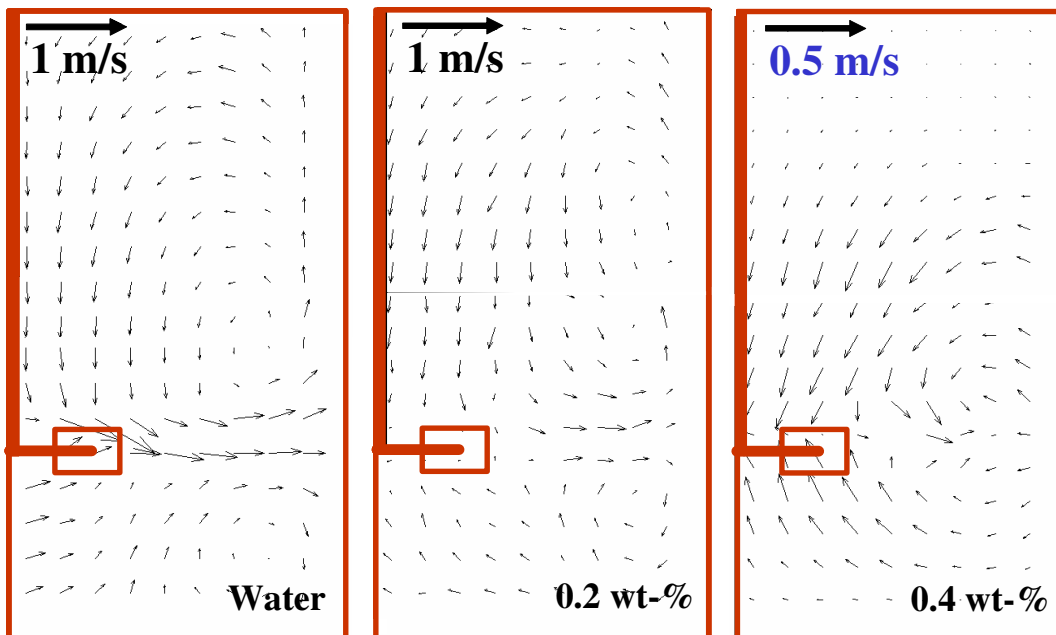
Figure 20b. PIV-results with increasing viscosity, 14 dm^3 vessel, impeller tip speed 1.35 m/s. Note the different vector scale with 0.4 wt-% xanthan. The 0.4 wt-% corresponds with CFD-simulation in Figure 19.

4.3 Vessel heterogeneity

Our simulations and measurements confirmed earlier findings; stirred G-L reactors are inherently heterogeneous in terms of mass transfer [V, VII, IX]. The magnitude of the heterogeneity was a surprise, in our simulations only 10% of the reactor volume accounted for 50% of the vessel mass transfer rate (Figure 21). This indicates that most of the reactor can be considered a 'dead-space' and it has little importance in terms of mass transfer. We were able to describe the formation of an impeller cavern and gas-slugs with shear-thinning fluids [VIII, IV] (Figure 22). In this thesis it was found out that to describe mass transfer area accurately the bubble breakage and coalescence need to be accounted for [III, IV, VII, VIII], modelling with a single bubble size was not accurate enough.
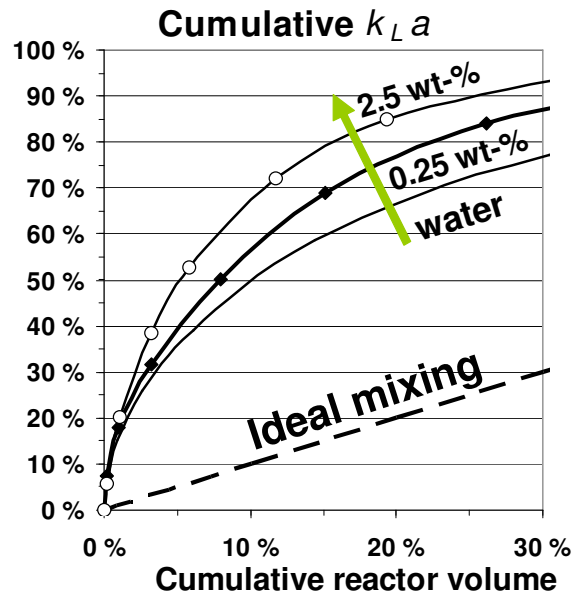
Figure 21. Cumulative k_La [%] vs. cumulative reactor volume [%]. Dashed line: ideal mixing, water (line), blocks (0.25 wt-%) and circles (2.5 wt-%), 390 rpm, 0.7 vvm. Heterogeneity grows with increasing viscosity (shown with arrow).
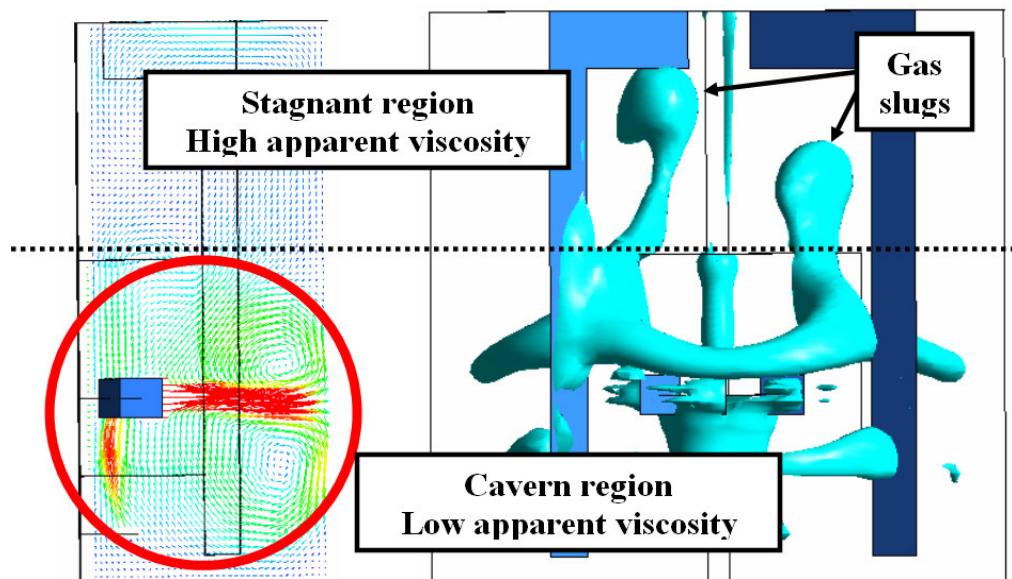
Figure 22. Cavern and gas-slug formation in 200 dm^3 vessel. 0.5 vvm, 390 rpm, constant bubble size 4 mm, 0.75 wt-% xanthan [IV].

To study the vessel heterogeneity in normal reactor scales instead of laboratory conditions, an industrial xanthan fermentation batch was simulated. The results show that there is a mass transfer limitation, since the reaction rate was significantly accelerated by improving the volumetric mass transfer rate. The results [V] indicate that the heterogeneity of the reactor can be decreased by suitable operation strategies during the batch run. With CFD long unsteady state simulations (>1 min real time) are not feasible. In publication [IV] the industrial reactor of 70 m^3 was simulated, the results revealed that there are local differences in concentrations and in the reaction rate. The differences were mainly caused by the hydrostatic pressure gradient, differences in local mass transfer rate and the convective flow fields inside the reactor. The mass transfer rate was massively over predicted due to the single bubble size assumption and a small bubble size based on laboratory scale measurements [IV]. BSDs vary considerably around different parts of the vessel [II, III], generating differences in local characteristic G-L areas. These findings suggest that a uniform bubble size should not be used. Larger bubbles are trapped in downward flows and in the centres of re-circulating flows. The smaller bubbles can be found in the impeller discharge region and in areas of low hold-up [II, VIII, IX]. It is obvious that in order to make detailed simulations of agitated G-L reactors the bubble size distribution needs to be modelled in detail.

4.4 Changing operating conditions and physical properties
In this work the studies began with dilute Newtonian G-L systems and moved gradually to complex systems mimicking bioreactors. The operating conditions were chosen in the end to be in line with typical industrial operating conditions (0.1-1.0 vvm, 0.1-3.0 W/kg). In G-L reactors there are multiple counteracting phenomena working at the same time, separating these effects is challenging and the analysis is not straightforward.

Increase in impeller speed results in increased liquid flow, enabling the vessel to trap more gas. In general, bubble size is decreased due to increased turbulent energy dissipation. The decreased bubble size reduces the slip-velocity of the bubbles resulting in larger hold-ups. A larger gas

hold-up means more bubble coalescence, resulting in the increased bubble size. In areas of downward flow and in the centres of re-circulating flows the bubbles tend to hover in a standstill, accumulating more gas and resulting in significantly increased bubble size. Correlations (Middleton, 1992; van't Riet, 1979) predict the decrease of bubble size with increasing agitation. However in real reactors the effect is not uniform throughout the vessel. There are even some locations where the effect is opposite to the prediction of the correlation (Figure 23). k_La is very sensitive to changes in bubble size and most of the mass transfer area is in small bubbles (Figure 24), so the hold-up increase does not necessarily lead to increase in the mass transfer rate. This may explain why the CJ and PJ impellers do not have a higher k_La in spite of higher vessel averaged gas hold-up.
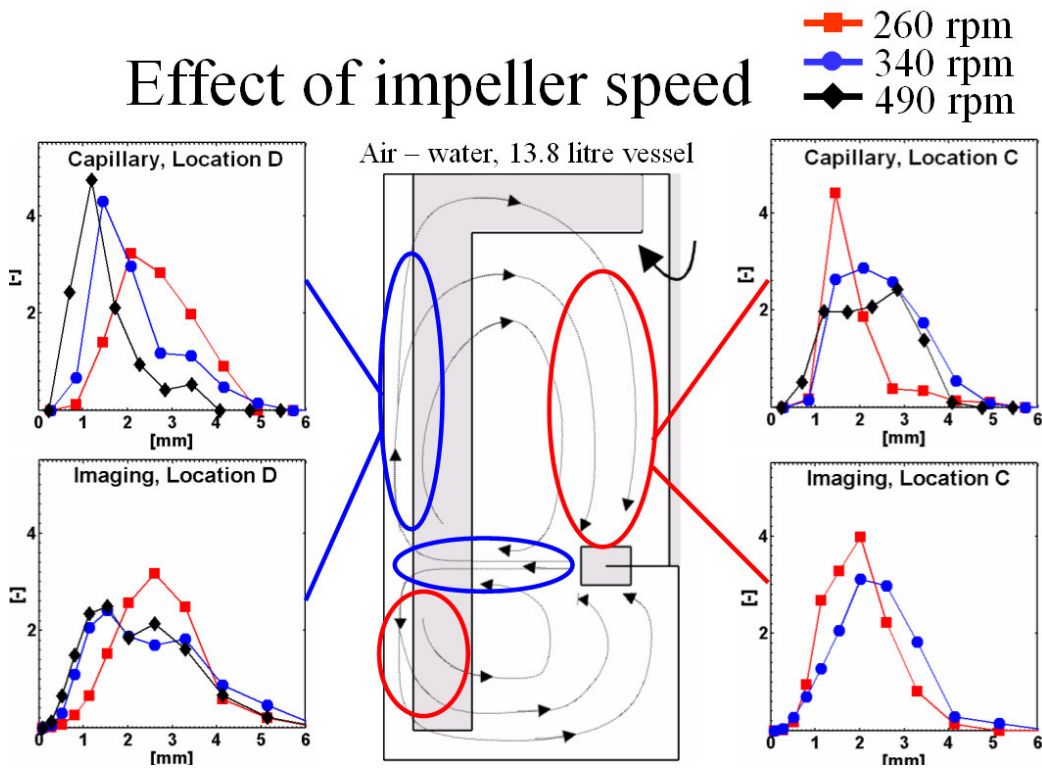
Figure 23. Bubble size distributions with DI and CSP at different parts of the vessel. Bubble size increases with agitation in areas of downward flow (Red) and decreases in other areas (Blue). 14 dm^3 vessel, RT [II].
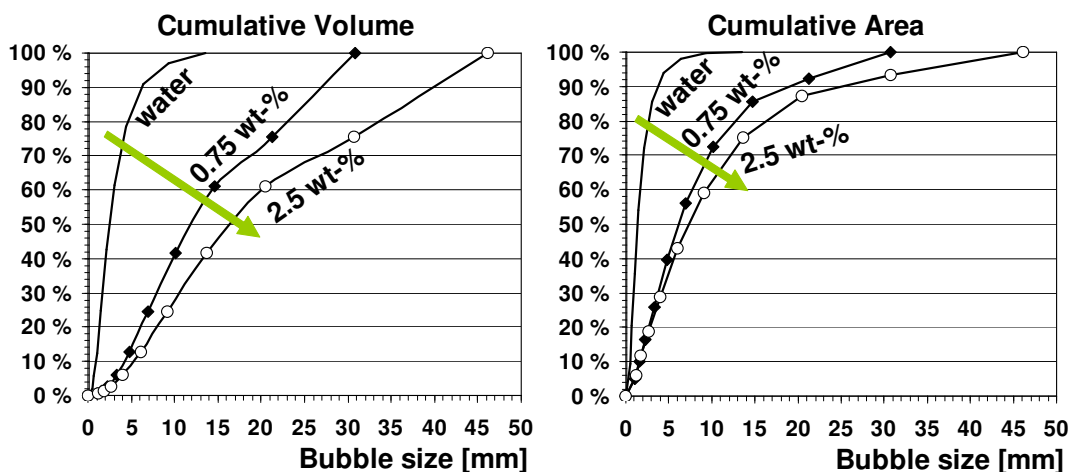
Figure 24. The simulated effect of increasing viscosity on cumulative volume and area distributions [VIII].

The effect of increased gassing rate seems straightforward: increasing gassing rate increases hold-up if the impeller does not flood. But, there are also competing phenomena. An increased hold-up means a decrease in impeller power and pumping numbers, which decreases hold-up. The bubbles coalesce more in a dense dispersion resulting in increased size and terminal velocity making them able to escape the reactor faster. The decrease in turbulent energy dissipation slightly reduces the mass transfer rate in the liquid film (k_L). In short, there even if the vessel averaged $k_L a$ increases with increased agitation and gassing, there are some locations in the vessel where the $k_L a$ actually decreases. The overall effect is a combination of several counteracting phenomenon and there are local changes that oppose the vessel averaged trend. If a reactor is modelled as ideally mixed it is a significant simplification and may result in an inadequate representation of the system.

The used models were constructed based on changes in physical properties. With CO_2-butanol and air-water dispersions [II, VI] the effects of interfacial surface tension and liquid density were evaluated. The butanol system exhibited a smaller bubble size and buoyancy, resulting in larger mass transfer areas. A model was developed which can describe both systems with good accuracy. A fitting with multiple systems is more reliable for describing new systems than a fitting based on just one system. In later publications [V, VIII] the effect of rising apparent viscosity and non-Newtonian behaviour was investigated in detail. The effect of increasing viscosity is of great importance, the mass transfer rate drops by over an order of magnitude when apparent viscosity rose from 0.001 to 40 Pa·s. With non-Newtonian fluids the vessel often separates into two parts: the well mixed cavern area and the stagnant bulk area. This phenomenon was correctly predicted in the simulations. An affiliated phenomenon is gas-slug creation: gas accumulates at the ceiling of the cavern, coalesces into larger bubbles or goes though the high viscosity layer in bubble swarms. Without a swarm correction or bubble coalescence the CFD-simulations categorically crashed due to gas accumulation in the reactor. In article [IV] we predicted a flooding impeller, but could not confirm this experimentally.

The developed model is usable for studying a wide range of G-L dispersions of varying physical properties. The ability to spot harmful phenomenon aids in troubleshooting, but the simulation results shouldn't be taken as quantitative values without some experimental backing. Trends gained from the simulation can help in discovering what way the reactor should be operated, or what difficulties are likely to occur.

4.5 Effect of impeller geometry

Experiments proved that vessel averaged volumetric G-L mass transfer rate is rather independent of vessel geometry. The total amount of turbulent energy dissipated in the reactor is the defining factor. Still, there were major differences in the G-L dispersions generated by the different impellers. For instance the experimental hold-up by RT / PJ were 6.5 / 8.8 vol-% with same operating conditions and the CFD simulations were able to predict the rising hold-up. The CFD-simulated local BSDs and flow patterns differ significantly with the impellers [IX]. The computational grids of the impellers are presented in Figure 25. The effect of impeller geometry in CFD simulations are compared against widely used correlations in Figure 26.
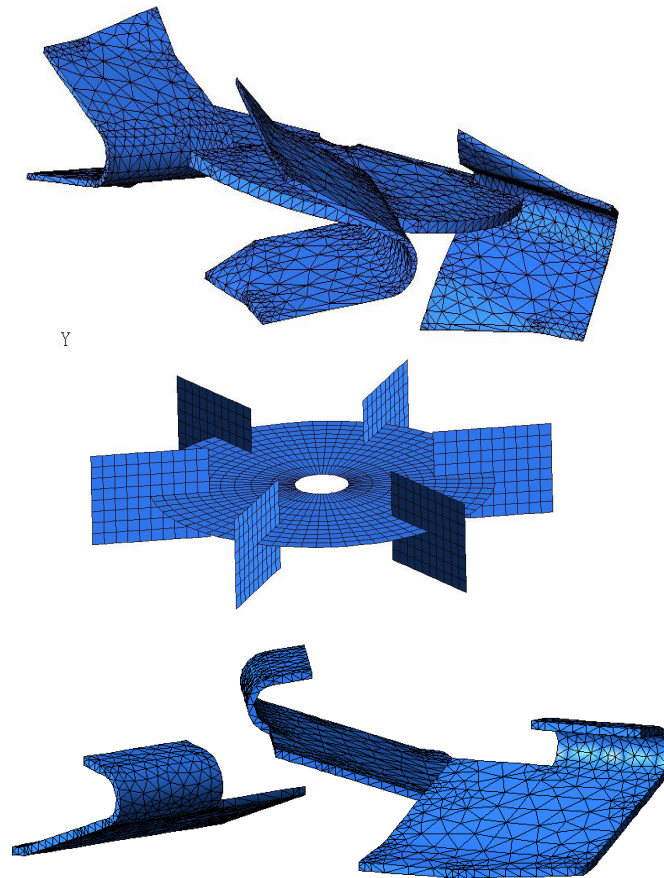
Figure 25. Surface grids for Phasejet (up), Rushton (middle) and Combijet (down). Note that some simplifications were made to the impeller geometries.
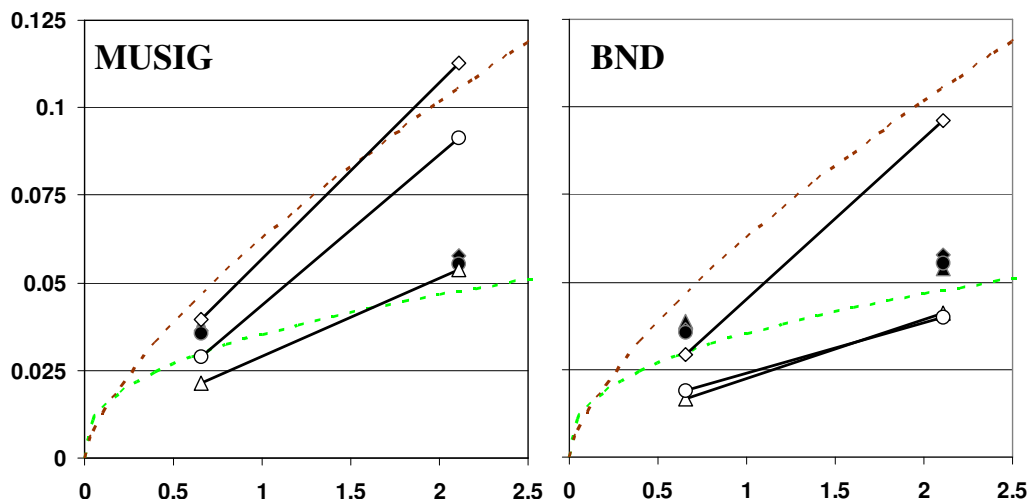
Figure 26. k_La [s^{-1}] vs. mixing intensity [W/kg] at constant 0.7 vvm gassing with different impeller geometries. Two popular correlations; Middleton (lower dashed line) and Van't Riet (upper dashed line) are compared against experiments. Experimental values in dark markers and simulations with open markers. CJ (parallelogram), PJ (circle), RT (triangle).

Popular semi-empirical mass transfer correlations of Middleton (1992) and van't Riet (1979) have a large deviation in their predictions. Middleton claims that his correlation includes the un-idealities of a stirred reactor and thus gives out higher predictions for the volumetric mass transfer rate. Both correlations do not take into account the vessel geometry, so the impeller geometry or vessel scale has no effect on the vessel averaged k_La. The experiments support this claim. When simulating the stirred vessel with CFD there are significant differences between BND and MUSIG simulations [IX]. The most accurate results are obtained with the Rushton turbine. This is not a surprising, since PB models and stirred tank simulations in general are validated on experimental results from RT-systems. Since, the experimental data is mostly available from one type of an impeller, it is reasonable to suspect that the developed PB models may not be as universal as claimed. The simulated k_La is affected by the miss predicted gas hold-up (PJ and CJ), which has a significant effect on the final results.

4.6 Combining CFD and multiblock-models
The multiblock model was used in several publications [III, V, VI, VII]. The advantages of multiblock models ultimately result from the faster computational time. This is caused by a smaller number of computational elements. The transparency and versatility of the used code is beneficial for academic purposes. Commercial CFD-codes do not share their models and numerical procedures, resulting in a 'black box' program with limited user customisation. In publications [III, V, VI] the multiblock model was used to fit parameters for bubble breakage and coalescence models. In publications [VI, VII] the multiblock model was compared against CFD simulations. CFD and multiblock models produced similar results, but the multiblock model was 1000-fold faster.

The full potential of the multiblock model was shown in publication [V] there dynamic batch bioreactor was simulated for several days, with detailed mass transfer, bioreaction and population balances. In Figure 27, local flow simulations are compared against a multiblock model. It can be seen that in the multiblock the local contrasts of the values are smoothed out,

but the general trend is very similar to the detailed flow simulation. However, the multiblock model requires detailed experimental data or CFD-simulations as a perquisite. The flowfields, turbulent energy dissipation and pressure gradients are needed for the generation of multiblock model. The manual generation of the multiblock model is a time consuming task, requiring detailed knowledge about the modelled system and good programming skills.
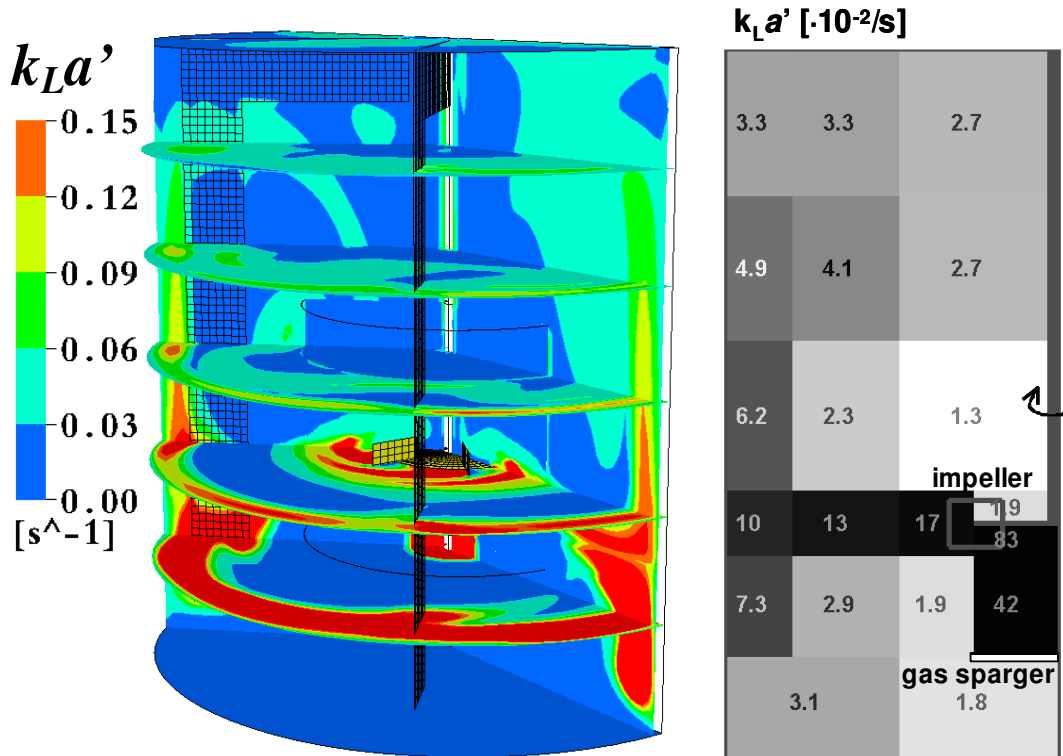
Figure 27. Local k_La's [s^{-1}] by local flow modelling and the multiblock model [VII]

4.7 Gas-Liquid mass transfer

In this work two approaches were applied: the complex model included transferring components in both phases with a detailed mass transfer model. This approach is fundamental, taking into account the concentration gradients in the liquid and gas phase, varying pressure, two-film theory and Maxwell-Stefan diffusion. This approach is computationally demanding and is mostly used with the multiblock model. In two occasions the rigorous mass transfer model was used with CFD [IV, VII]. The findings show that when dealing with slightly soluble gasses the effect of using the iterative two-film theory was minute [VII].

When dealing with poorly soluble gasses, no chemical reaction and small differences in the diffusivities of the components, it is reasonable to use a simple approach for mass transfer modelling. In publications [VIII, IX] oxygen was not modelled as a transferring component. The local volumetric mass transfer coefficient (k_La) is calculated from local gas-liquid area and local k_L, without the actual driving force of concentration difference from equilibrium. This rough vessel averaged k_La can be used in simpler reactor models, which require far less computational effort.

5. CONCLUSIONS

No single bubble size measurement technique can describe the BSD in all conditions [II]. Different measurements techniques often yield contradicting results. The technique needs to be selected so that it covers a wide range of the bubble size range and at the same time is usable at realistic reactor operating conditions. Presentation of the results is of great importance and should not be neglected. Obtaining statistically relevant BSDs from viscous solutions manually was unfeasible because of a wide size distribution ~0.1 … 50mm [VIII]. A new imaging method was developed measure local mixing times [VIII].

The traditional assumption of an ideally mixed vessel often fails to describe a reactor in required detail [VII]. Gas slug creation and dead-spaces are common phenomenon in bioreactors, and can't be described by models with an ideally mixed assumption. More spatial detail can be gained by using CFD or multiblock modelling at the expense of computational cost. CFD has become widely used as a design tool, but it is still unable to fit model parameters and make long transient simulations. In our work we constructed a computationally lighter multiblock model based on the CFD-simulated flow-fields, energy dissipations and pressure gradients. Complex model parameters like bubble breakage and coalescence were fitted in the multiblock model and then verified in the detailed CFD-simulations. It was shown that the multiblock model offers an optimal trade-off between computational time and modelling accuracy [V, VI, VII]. A multiblock model was constructed from several pseudo steady-state solutions and then used to simulate two day batch fermentation with changing physical properties [V]. It was shown that commercial xanthan production has a mixing and mass transfer limitation.

One phase CFD-modelling has been extensively validated for Newtonian fluids at the turbulent and laminar flow regimes. However, there are many difficulties when modelling turbulence at the transitional turbulent regime. One phase simulations proved that RANS modelling overestimates the mixing time at peripheral areas [VIII]. Variables that are known to be poorly predicted with coarse computational grids (i.e. turbulent energy dissipation) can be corrected by scaling with the experimental value (mechanical energy input). The computational time is vital when using population balances and other complex phenomenological models.

Models need to be validated in wider range vessel geometries and operating conditions to be reliable in scale-up. It seems that RT simulations produced more accurate results than novel impeller geometries. Currently it is not feasible to make complex simulations that include all the physical phenomena, because their magnitude can not be verified and fitted accurately (e.g. swarm interactions, turbulent slip-velocity dampening, and non-drag interfacial forces). It is important to recognise and accept the uncertainties in modelling and act accordingly; G-L mass transfer in stirred tanks is so complex that it needs to be grounded on experimental measurements trough parameter fitting. As a summary it can be said that gas-liquid modelling still needs a lot of improvements to be reliable without experimental verification.

My goal was to identify the important sub-models that need to be taken into account in order to successfully model large non-Newtonian bioreactors. It was shown that gas-liquid mass transfer in stirred vessels can be simulated successfully with a relatively small number of essential sub-models: bubble drag, viscosity, k_L, bubble- breakage and coalescence models. Many viscosity and drag models were tested and they all performed reasonably well. The most important thing to model correctly is the local bubble size; it influences the gas hold-up through bubble slip velocity and controls the interfacial area. The BSD in stirred vessels is wide, majority of the mass transfer area is in small bubbles whereas the gas volume is in larger ones, and hence both need to be modelled adequately. The bubble size discretisation needs to be dense with small bubbles and needs to cover a wide bubble size range [VIII]. We were able to predict gas hold-up and G-L mass transfer rates in a wide range of viscosities, vessel geometries and operating conditions. Gas slug creation and cavern formation were also captured in the simulations with viscous fluids. Mass transfer in stirred reactors appears to be very heterogeneous: 50% of the Gas-Liquid mass transfer took place in just 10% of the reactor volume [VIII]. This thesis provides the building blocks (sub-models) for an aerobic bioreactor simulation and insight on how to use them.

NOTATION

a	interfacial area (m^2/m^3(liquid))
A	a geometry related constant in eq. 49 (-)
A_h	projected surface-area (m^2)
c	concentration (wt-% or mg/L)
c^*	equilibrium concentration (mg/L)
C_μ	a constant in the k-ε model
C_{1-6}	model parameters
C_D	bubble drag coefficient (-)
D	diameter (m)
D_L	liquid phase diffusion coefficient (m^2/s)
d	characteristic bubble group size (m)
d_{32}	Sauter mean diameter $= \Sigma d^3 / \Sigma d^2$ (m)
E(d)	bubble aspect ratio (-)
f	breakage volume fraction (-)
g	acceleration due to gravitation (m/s^2)
$g(d_k)$	breakage frequency, s^{-1}
G	geometric ratio (-)
$h(d_k, d_p)$	coalescence frequency (m^3/s)
k, p, i	index numbers
k	kinetic energy (J/kg)
K	consistency index (($kg \cdot s^{-2}$)/m)
K	a bubble swarm model parameter in eq. 42 (-)
k_L	mass transfer coefficient in liquid film (m/s)
$k_L a$	volumetric mass transfer coefficient (s^{-1})
M	momentum transfer term
Mo	Morton number, eq. 41 (-)
n	flow index (-)
n	bubble number density (m^{-3})
n(d)	number density, eq. 47 (-)
N	impeller rotation speed (s^{-1})
N	number of bubbles, eq. 47-48 (-)
p	pressure (Pa)
$r_{O2,CO2}$	reaction rate (mol/L/h)
$r_{b,x,s,n}$	reaction rate (g/L/h)
Re_{imp}	Impeller Reynolds number, eq. 16 (-)
Re	bubble Reynolds number, eq. 39 (-)
t	time (s)
u	velocity (m/s)
U_{slip}	bubble slip-velocity (m/s)
v	velocity (m/s)
v(d)	volume density, eq. 48 (-)
V	volume (m^3)
We	Weber number, eq. 26 (-)
S	source / sink term ($m^{-3}s^{-1}$)

Greek letters

α	volume fraction (-)
$\beta(d_k,d_p)$	probability that bubble of size d_k is formed when d_p breaks (m^{-1})
γ	shear rate (s^{-1})
ε	turbulent energy dissipation (W/kg(liquid))
μ	viscosity (Pa•s)
σ	surface tension (N/m)
θ	temperature (ºC)
ρ	density (kg/m^3)
η	coalescence efficiency (-)
τ	yield stress (Pa)
λ	viscosity model parameter (s)
ξ	ratio of minimum eddy size and bubble size (-)
$\lambda(d_k,d_p)$	coalescence efficiency (-)

Abbreviations

BND	bubble number density
BSD	bubble size distribution
CFD	computational fluid dynamics
CJ	combijet
CSP	capillary suction probe
CSTR	continuous stirred tank reactor
DI	digital imaging
DNS	direct numerical simulation
DO	dissolved oxygen
G	gas
L	liquid
LDA	laser Doppler anemometry
LES	large eddy simulation
MFOR	multiple frames of reference
MUSIG	multiple size group
NC	number of classes
PB	population balance
PDA	phase Doppler anemometry
PIV	particle imaging velocimetry
PJ	phasejet
RANS	Reynolds averaged Navier-Stokes
RSM	Reynolds stress model
RT	Rushton turbine
SST	shear stress transport
VLE	vapour-liquid equilibrium
vvm	volume of gas feed per liquid volume in minute (m^3(gas)/(m^3(liquid)·min))

Subsricpts

0	at zero / initial
20	at 20 Cº
app	apparent

b	biomass
BR	breakage
bub	bubble
C	continuous
CO	coalescence
CR	critical
D	dispersed
disp	dispersion force
drag	drag force
eddy	eddy viscosity
if	interfacial
imp	impeller
lift	lift force
mass	added mass force
max	maximum
min	minimum
n	nutrient source
s	carbon source
tot	total
x	xanthan

REFERENCES

Adrian, R.J., Twenty years of particle image velocimetry. *Experiments in Fluids* **2005**, *39,* 159–169.

Alopaeus, V.; Koskinen, J.; Keskinen, K.I.; Majander, J. Simulation of the population balances for liquid-liquid systems in a nonideal stirred tank. Part 2 - parameter fitting and the use of the multiblock model for dense dispersions. *Chem. Eng. Sci.* **2002**, *57(10)*, 1815-1825.

Alves, S.S., Maia, C.I., and Vasconcelos, J.M.T. Experimental and modelling study of gas dispersion in a double turbine stirred tank, *Chemical Engineering Science* **2002***, 57,* 487-496.

Amanullah, A.; Hjotrh, S.A.; Nienow, A.W. A new mathematical model to predict cavern diameter in highly shear thinning power law fluids using axial flow impellers. *Chemical Engineering Science* **1998a**, *53(3)*, 455-469.

Amanullah, A.; Carreron-Serrano, L.; Castro, B.; Galindo, E.; Nienow, A.W. The influence of impeller type in pilot scale xanthan fermentations. *Biotechnology and Bioengineering* **1998b,** *57(1)*, 95-108.

Bakker, A.; van den Akker, H.E.A. A computational model for the gas - liquid flow in stirred reactors. *Chemical Engineering Research and Design* **1994**, *72(A4)*, 594-606.

Barigou, M.; Greaves, M. Bubble size in the impeller region of a Rushton turbine, *Trans. IChemE.* **1992a**, *70A*, 153-160.

Barigou, M.; Greaves, M. Bubble-size distributions in a mechanically agitated gas-liquid contactor, *Chem. Eng. Sci.* **1992b**, *47*, 2009-2025.

Bird, R.B, Stewart, W.E; Lightfoot, E.N. *Transport phenomena*, **1960**, Wiley.

Bisio, A.; Kabel, R. *Scaleup of chemical processes*, **1985**, Wiley.

Cabaret, F; Fradette, L; Tanguy, P.A. Characterization of macro-mixing kinetics using advanced image-analysis. *12th European Conference on Mixing (Bologna)* **2006**, 391-398.

Chhabra, R.P. *Bubbles, Drops, and Particles in Non-Newtonian Fluids 2nd edition*, **2007**, CRC press, 771p.

Chhabra, R.P. Rising velocity of a swarm of spherical bubbles in power law fluids at high Reynolds numbers, *The Canadian Journal of Chemical Engineering* **1998**, *76*, 137-140.

Chigier, N. Optical imaging of sprays. *Progress in Energy and Combustion Science* **1991**, *17(3)*, 211-62.

Chesters, K.A. The modelling of coalescence processes in fluid-liquid dispersions: A Review of current understanding. *Chemical Engineering Research and Design* **1991**, *69*, 259-270.

Clift, R. Grace, J.R.; Weber, M.E. *Bubbles, Drops, and Particles*, **2005**, Dover, 381 p.

Coulaloglou, C.A.; Tavlarides, L.L. Description of interaction processes in agitated liquid-liquid dispersions. *Chemical Engineering Science* **1977**, 32, 1289-1297.

Garcia-Ochoa, F.; Santos, V.E.; Alcon, A. Metabolic structured kinetic model for xanthan production. *Enzyme and Microbial Technology* **1998**, *23(1/2)*, 75-82.

Garcia-Ochoa, F.; Gomez, E.; Santos, V.E. Oxygen transfer and uptake rates during xanthan gum production. *Enzyme and Microbial Technology* **2000**, *27*, 680-690.

Gogate, P.R.; Beenackers A.A.C.M.; Pandit, A. Multiple-impeller systems with a special emphasis on bioreactors: a critical review. *Biochemical Engineering Journal* **2000**, *6*, 109-143.

Hartmann, H.; Derksen, J.J.; Akker, H.E.A. Mixing times in a turbulent stirred tank by means of LES. *AIChE Journal* **2006**, 52(11), 3696-3706.

Hartmann, H. *Detailed simulations of liquid and solid-liquid mixing, turbulent agitated flow and mass transfer (PhD thesis)*, **2005**, Delft university press. 187 p.

Hristov, H.; Mann, R.; Lossev, V.; Vlaev, S.D.; Seichter, P. A 3-D anlysis of gas-liquid mixing, mass transfer and bioreaction in stirred bio-reactor. *Trans. Ichem. E.* **2001**, *79C*, 232-241.

Jackson, M.L; Shen, C-C. Aeration and mixing in deep tank fermentation systems. *AIChE Journal* **1978**, *24*, 63-71.

Kawase, Y.; Halard, B.; Moo-Young, M. Liquid-phase mass transfer coefficients in bioreactors. *Biotechnology and Bioengineering* **1992**, *39(11)*, 1133-1140.

Kerdouss, F.; Bannari, A.; Proulx, P. CFD modeling of gas dispersion and bubble size in a double turbine stirred tank**,** *Chem. Eng. Sci.* **2006**, *61(10)*, 3313-3322.

Laakkonen, M. *Development and validation of mass transfer models for the design of agitated gas-liquid reactors (PhD thesis)*, (http://lib.tkk.fi/Diss/2006/isbn9512284618), **2006**, Espoo.

Lane, G.L. *Computational Modelling of Gas-Liquid Flow in Stirred Tanks (PhD. Thesis)*, http://www.newcastle.edu.au/service/library/adt/public/adt-NNCU20070712. 140253/index.html, **2006**, University of Newcastle.

Lane, G.L.; Schwarz, M.P.; Evans, G.M. Numerical modelling of gas-liquid flow in stirred tanks, *Chem. Eng. Sci.* **2005**, *60(8-9)*, 2203-2214.

Lehr, F.; Millies, M.; Mewes, D. Bubble-size distributions and flow fields in bubble columns, *AIChE Journal.* **2002**, *48*, 2426-2443.

Li, H.Z. Bubbles in non-Newtonian fluids: Formation, interactions and coalescence. *Chemical Engineering Science* **1999**, *54*, 2247-2254.

Lo, S. Application of population balance to CFD modeling of gas-liquid reactors. *Trends in Numerical and Physical Modelling for Industrial Multiphase Flows* (Corse, France), **2000**.

Luo, H.; Svendsen, H.F. Theoretical model for drop and bubble breakup in turbulent dispersions, *AIChE Journal.* **1996**, *42*, 1225-1233.

Machon, V., Vlcek, J., Nienow, A.W., Solomon, J. Some effects of pseudoplasticity on hold-up in aerated, agitated vessels. *Chem. Eng. J.* **1980**, *19*, 67-74.

Margaritis, A.; te Bokkel, D.W.; Karamanev, D.G. Bubble Rise Velocities and Drag Coefficients in Non-Newtonian Polysaccharide Solutions. *Biotechnology and Bioengineering* **1999**, *64 (3)*, 257-263.

Middleton, J.C. Gas-liquid dispersion and mixing, in: *Mixing in the Process Industries*, Harnby, N., Edwards, M.F., Nienow, A.W. (eds), **1992**, Butterworth-Heinemann, Oxford.

Miyahara, T.; Yamanaka, S. Mechanics of motion and deformation of a single bubble rising through quiescent highly viscous Newtonian and non-Newtonian media, *Jour. Chem. Eng. Jap.* **1993**, *26*, 297-302.

Nienow, A.W.; Elson, T.P. Aspects of mixing rheologically complex fluids. *Chemical Engineering Research and Design* **1988**, *66*, 5-15.

Paul, E.; Atiemo-Obeng, V.; Kresta, S. *Handbook of industrial mixing*, **2004**, Wiley.

Ranade, V.V., *Computational Flow Modeling for Chemical Reactor Engineering*, **2002**, Academic Press.

Schügerl, K.; Bellgardt, K.H. *Bioreaction Engineering, Modeling and Control*, **2000**, Springer Verlag, Berlin.

Tabib, M.V.; Roy, S.A,; Joshi, J.B. CFD simulation of bubble column – An analysis of interphase forces and turbulence models, *Chem. Eng. Jour.* **2007**, doi:10.1016/j.cej.2007.09.015

Tzounakos, A.; Karamanev, D.G.; Margaritis, A.; Bergougnou, M.A. Effect of the surfactant concentration on the rise of gas bubbles in power-law non-Newtonian liquids, *Ind. Eng. Chem. Res.* **2004**, *43*, 5790-5795.

Uusi-Kyyny, P.; Pokki, J-P.; Laakkonen, M.; Aittamaa, J.; Liukkonen, S. Vapor liquid equilibrium for the binary systems 2-methylpentane + 2-butanol at 329.2 K and n-hexane + 2-butanol at 329.2 and 363.2 K with a static apparatus. *Fluid Phase Equilib.* **2002**, *201*, 343-358.

Van't Riet, K. Review of measuring methods and results in nonviscous gas-liquid mass transfer in stirred vessels, *Ind. Eng. Chem. Proc. Des. Dev.* **1979**. *18(3)*, 357-64.

Venneker, B. *Turbulent Flow and Gas Dispersion in Stirred Vessels with Pseudoplastic Liquids (PhD thesis)*. **1999**, University of Delft.

Visuri, O.; Laakkonen, M.; Aittamaa, J. A digital imaging technique for the analysis of local inhomogeneities from agitated vessels. *Chemical Engineering & Technology* **2007**, *30(12)*, 1692-1699.

Vlaev, D.; Mann, R.; Lossev, V.; Vlaev, S.D.; Zahradnik, J.; Seichter, P. Makro-mixing and streptomyces fradiae modelling oxygen and nutrient segregation in a industrial bioreactor. *Trans IchemE.* **2000**, *78A*, 354-362.

van Wachem, B.G.M.; Almstedt, A.E. Methods for multiphase computational fluid dynamics, *Chem. Eng. Jour.* **2003**, *96*, 81-98.

Westerweel, J. Fundamentals of digital particle image velocimetry. *Measurement Science & Technology* **1997**, *8(12)*, 1379-1392.

Wu, Q.; Kim, S.; Ishii, M.; Beus, S.G. One-group interfacial area transport in vertical bubbly flow, *Int. J. Heat Mass Transfer* **1998**, *41(8-9)*, 1103-1112.

Yaseen, E. I.; Herald, T. J.; Aramouni, F. M.; Alavi, S. Rheological properties of selected gum solutions**.** *Food Research International* **2005**, *38(2)*, 111-119.